

# Homosalate boosts the release of tumour-derived extracellular vesicles with protection against anchorage-loss property

Eleonora Grisard<sup>1</sup>  | Nathalie Nevo<sup>1</sup>  | Aurianne Lescure<sup>2</sup> | Sebastian Doll<sup>3</sup>  |  
 Maxime Corbé<sup>2</sup> | Mabel Jouve<sup>4</sup>  | Gregory Lavieu<sup>1,5</sup>  | Alain Joliot<sup>1</sup>  |  
 Elaine Del Nery<sup>2</sup>  | Lorena Martin-Jaular<sup>1</sup>  | Clotilde Théry<sup>1</sup> 

<sup>1</sup>Institut Curie, PSL Research University, INSERM U932, Paris, France

<sup>2</sup>Institut Curie, PSL Research University, Translational Research Department, BioPhenics Platform, PICT-IBISA, Paris, France

<sup>3</sup>Institute of Metabolism and Cell Death, Helmholtz Zentrum München, Neuherberg, Germany

<sup>4</sup>Institut Curie, PSL Research University, CNRS UMR3215, Paris, France

<sup>5</sup>Université Paris Cité, INSERM U1316, CNRS UMR 7057, Paris, France

## Correspondence

Clotilde Théry, Institut Curie, PSL Research University, INSERM U932, Paris, France.  
 Email: [clotilde.thery@curie.fr](mailto:clotilde.thery@curie.fr);  
 Lorena Martin-Jaular, Institut Curie, PSL Research University, INSERM U932, Paris France  
 Email: [lorena.martin-jaular@curie.fr](mailto:lorena.martin-jaular@curie.fr)

Lorena Martin-Jaular and Clotilde Théry are co-last and co-corresponding authors.

## Abstract

Eukaryotic cells, including cancer cells, secrete highly heterogeneous populations of extracellular vesicles (EVs). EVs could have different subcellular origin, composition and functional properties, but tools to distinguish between EV subtypes are scarce. Here, we tagged CD63- or CD9-positive EVs secreted by triple negative breast cancer cells with Nanoluciferase enzyme, to set-up a miniaturized method to quantify secretion of these two EV subtypes directly in the supernatant of cells. We performed a cell-based high-content screening to identify clinically-approved drugs able to affect EV secretion. One of the identified hits is Homosalate, an anti-inflammatory drug found in sunscreens which robustly increased EVs' release. Comparing EVs induced by Homosalate with those induced by Bafilomycin A1, we demonstrate that: (1) the two drugs act on EVs generated in distinct subcellular compartments, and (2) EVs released by Homosalate-, but not by Bafilomycin A1-treated cells enhance resistance to anchorage loss in another recipient epithelial tumour cell line. In conclusion, we identified a new drug modifying EV release and demonstrated that under influence of different drugs, triple negative breast cancer cells release EV subpopulations from different subcellular origins harbouring distinct functional properties.

## 1 | INTRODUCTION

Extracellular Vesicles (EVs) are membrane enclosed particles secreted by all types of cells. Given that EVs can transport nucleic acids, proteins and lipids, they are fundamental means of inter-cellular communication (Cocozza, Grisard, Martin-Jaular, Mathieu, & Théry, 2020; van Niel, D'Angelo, & Raposo, 2018). EVs can originate in different locations within cells: exosomes originally form as intraluminal vesicles (ILVs) of multivesicular bodies (MVBs) along the endocytic pathway, whereas ectosomes (or microparticles) are generated by direct budding away from the plasma membrane (PM). Exosomes have the same diameter range as ILVs, that is, 50–150 nm, but PM-derived ectosomes, different EVs originating from other compartments (e.g., recycling endosomes), and even some particles released by virus-infected or apoptotic cells can also be in the same size range (Cocozza et al., 2020; Nolte-T Hoen, Cremer, Gallo, & Margolis, 2016). By contrast, only ectosomes, oncosomes and apoptotic bodies can be larger (up to 5 µm in diameter) (Minciacchi, Freeman, & Di Vizio, 2015). Importantly, different EVs present different combinations of protein markers, as revealed by comparative proteomic studies (Jeppesen et al., 2019; Kowal et al., 2016; Zhang et al., 2018), and consequently could have distinct functional properties (Imjeti et al., 2017; Tkach & Théry, 2016; Willms, Cabañas, Mäger, Wood, & Vader, 2018). In particular, EVs released by cancer cells can play opposite roles in cancer progression

This is an open access article under the terms of the [Creative Commons Attribution-NonCommercial-NoDerivs License](https://creativecommons.org/licenses/by-nc-nd/4.0/), which permits use and distribution in any medium, provided the original work is properly cited, the use is non-commercial and no modifications or adaptations are made.

© 2022 The Authors. *Journal of Extracellular Vesicles* published by Wiley Periodicals, LLC on behalf of the International Society for Extracellular Vesicles.

(Willms et al., 2018). For example, EVs released by breast cancer cells have been shown to display pro-metastatic properties (Fong et al., 2015; Kia, Mortazavi, Paryan, Biglari, & Mohammadi-Yeganeh, 2019), similar to those released by pancreatic cancer (Costa-Silva et al., 2015), prostate cancer (Ciardiello et al., 2019) or liver cancer (Fang et al., 2018). Conversely, other studies have reported a protective role of EVs against cancer progression (Plebanek et al., 2017; Wolfers et al., 2001).

Isolating and studying individual EV subtypes is therefore crucial. Yet, current EV isolation techniques achieve only a partial separation of EV subtypes, although combinations of one or more techniques can considerably improve the distinction between EV subpopulations (Cocozza et al., 2020). The tetraspanins CD63 and CD9 are often used independently as exosome markers. However, they have preferential (but not exclusive) subcellular locations: CD63 is mostly localized in MVBs and consequently more enriched in exosomes, whereas CD9 is mostly localized at the PM and thus more enriched in ectosomes (Mathieu et al., 2021), although they can also be expressed simultaneously on the same EVs (Kowal et al., 2016). Using fluorescent tags to label EV markers (e.g., CD63 or CD9 tetraspanins) can help to study separately the biogenesis mechanisms of EVs containing those markers (Bebelman et al., 2020; Mathieu et al., 2021). As an alternative to fluorescent tags, also enzymatic tags can be used to label EVs, like luciferase enzymes (Lázaro-Ibáñez et al., 2021). In particular, Nanoluciferase (Nluc) has been successfully used to tag CD63 positive EVs (Cashikar & Hanson, 2019).

Here, we tagged CD63 or CD9 (Mathieu et al., 2021) with the Nluc enzyme to separately study two populations of EVs (CD63-positive and CD9-positive) released by MDA-MB-231 triple negative breast cancer cells. We then set-up a cell-based high-content screening (HCS) assay to detect the secretion of Nluc-CD63 or Nluc-CD9 tagged EVs by quantifying Nluc activity in the supernatant of cells. HCS methods are extensively used to rapidly identify small molecules with potential biological functions, and are of special interest for repurposing drug applications when performed using chemical libraries compounds already approved by regulatory agencies (FDA, EMA ...) (Macarron et al., 2011). Here, by screening an FDA- and EMA-drug library (Prestwick Chemicals V3), we found that Homosalate acts as a booster of EV secretion in MDA-MB-231 and other tumour cell lines.

We found that Homosalate and Bafilomycin A1, which had been shown to increase the secretion of MVB- derived EVs (= exosomes) by increasing MVB internal pH (Bowman, Siebers, & Altendorf, 1988; Edgar, Manna, Nishimura, Banting, & Robinson, 2016; Eitan, Suire, Zhang, & Mattson, 2016), act on distinct subcellular compartments. Homosalate specifically increased the release of an EV subpopulation enriched in a combination of SLC3A2/CD98, CD40 and CD9 markers. Importantly, we showed that, when applied on recipient tumour cells, EVs released by MDA-MB-231 cells upon treatment with Homosalate, but not Bafilomycin A1, increased migratory ability and conferred resistance to stress induced by anchorage loss. In conclusion, a novel multi-drug HCS assay for EVs' release allowed the identification of a novel drug able to increase the secretion of a specific EV subpopulation displaying specific functional properties.

## 2 | RESULTS

### 2.1 | Nanoluciferase tagged CD63 and CD9 are secreted into EVs

Our first goal was to develop a quantitative HCS assay to enable consistent and easy read-out of EV secretion in miniaturized 96- and 384-cell culture plate format. We fused two of the most common EV markers, CD63 and CD9 to the highly sensitive enzyme Nluc to monitor EV release from cells stably-expressing these fusion proteins. To minimize potential interference, Nluc was fused at the N-terminal end of human CD63 or CD9 (Bonsergent et al., 2021), away from the C-terminal lysosome-targeting signal of CD63 (Rous et al., 2002) (Figure 1A). Nluc is small but exceptionally bright (Hall et al., 2012), making it ideal for the quantification of EV secretion, in particular from small amounts of cells. In a bulk population of Nluc-CD63-transfected MDA-MB-231 triple negative breast cancer cells, we observed that Nluc activity was detectable from 390 cells and in the conditioned medium (i.e., supernatant) of 1,560 cells after 24 h (Figure 1A). Thus, we generated stable clonal populations of MDA-MB-231 expressing Nluc-CD63 or Nluc-CD9. For each cell line, we selected a clone with high Nluc activity (clone 7 for Nluc-CD63 and clone 3 for Nluc-CD9: around  $10^8$  luciferase activity/ 25,000–30,000 cells), and reliable detection in supernatant (Figure 1B). For both clones, comparable ratios of supernatant versus cells Nluc activity were observed (6%, Figure 1B). Analysis of the distribution of CD9 and CD63 in these two clones showed no major difference as compared to the parental MDA-MB-231 cell line, CD9 being detected at the plasma membrane and peripheral membranes, and CD63 enriched in large internal compartments (Figure 1C). Next, we determined for the two clones, the precise contribution of EVs in the total Nluc activity detected in the supernatant. Size Exclusion Chromatography (SEC) was used to separate released EVs which do not enter the pores of the gel and are eluted first (Böing et al., 2014), from soluble proteins that are the main source of potential contaminating Nluc activity in our system. To accurately characterize the content of each SEC fraction, we compared particle number, protein concentration and Nluc activity from fraction 7 (F7, first fraction post-void volume of the column) to F24. As shown in Figure 1B and 1C, for both cell lines, particle concentration measured by Nanoparticle Tracking Analysis (NTA) peaked in F9-11, although some particles were still detectable until F16-17 (red line in upper panel), indicating that they were present also in later fractions than in the predicted F7-11. Proteins were detectable from F14 on, with a peak in F20-21 (green line in upper panel), confirming a minimal overlap with EV-enriched fractions. The distribution of Nluc-activity (Figure 1B-C, blue line) closely overlapped with particle concentration distribution,

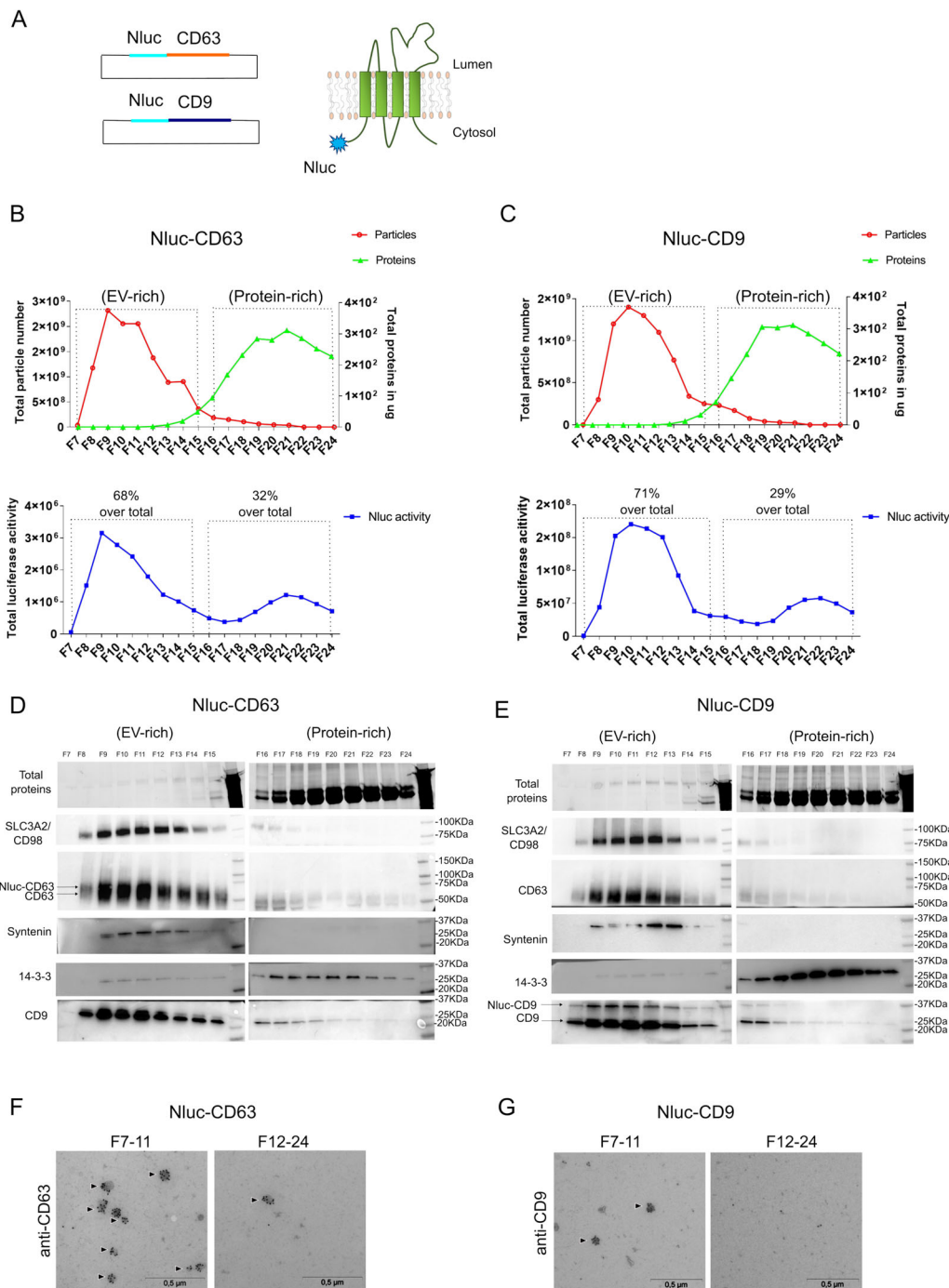


**FIGURE 1** Nanoluciferase tagged CD63 and CD9 are secreted into EVs. (A) Left: scheme of Nluc-CD63 and Nluc-CD9 plasmid constructs. Nluc enzyme was cloned into CD63 or CD9 encoding plasmids at the N-terminal position. Right: scheme of the topology of a tetraspanin (CD63 or CD9) with N-terminal Nluc-tag. (B) and (C) Measurement of total particle number (red line) by Nanoparticle Tracking Analysis (NTA), total protein in  $\mu\text{g}$  (green line) by BCA and total Nluc activity (blue line) in all single  $500\mu\text{l}$  SEC fractions from F7 to F24 recovered from Nluc-CD63 or Nluc-CD9 supernatants. Shown data are from a single pilot experiment. (D) and (E) Western Blot analysis of SLC3A2/CD98, CD63, Syntenin, 14-3-3 and CD9 markers in SEC fractions from Nluc-CD63 and Nluc-CD9 cells. Arrows indicate chimeric (Nluc-tagged) versus endogenous CD63 (D) or CD9 (E). (F) and (G) Representative TEM images showing CD63+ EVs (for Nluc-CD63) or CD9+ EVs (for Nluc-CD9) isolated from  $7 \times 10^6$  cells in F7-11 versus F12-24. Scale bar  $0.5\mu\text{m}$ . Shown data are from a single pilot experiment. Arrowheads indicate EVs positive for CD63 staining (F) or CD9 staining (G)

with a peak in F9-11 and F16-17. Interestingly, a smaller peak was detected in F21-22 corresponding to the peak of free proteins, indicating that a tiny portion of Nluc activity source is free in the supernatant or associated to very small membrane-derived objects (Figure 1B-C). According to these observations, we defined “EV-rich” fractions F7-15 and “Protein-rich” fractions F16-24. In this pilot experiment, we calculated the percentage of Nluc activity in EV-rich (F7-15) and Protein-rich (F16-24) over the total Nluc-activity detected in all fractions (F7-24). We determined that 68% and 71% of the total Nluc activity were associated to EV-rich fractions from Nluc-CD63 and Nluc-CD9 cells, respectively (Figure 1B-C). Conversely, protein-rich fractions were the source of Nluc activity for only 32% or 29% of the total Nluc activity in Nluc-CD63 (Figure 1B) and Nluc-CD9 (Figure 1C), respectively. To further confirm EV specific enrichment in the fractions F7-15 we checked by Western Blot the presence of EV markers in each SEC fraction from Nluc-CD63 and Nluc-CD9 clones. As expected, proteins were highly enriched in “Protein-rich” F16-24 and barely detectable in “EV-rich” F7-15 (Figure 1D-E). Importantly, EV markers SLC3A2/CD98 (<http://exocarta.org/index.html>) (Mathieu et al., 2021), CD63, CD9 and Syntenin were mainly enriched in F8-15 with peaks in F9, F10 and F11, consistent with previous findings (Figure 1B-C). Conversely, 14-3-3, a protein commonly identified in sEVs recovered by ultracentrifugation (<http://exocarta.org/index.html>) but recently defined as non-exosomal marker (Jeppesen et al., 2019) was found at low level in F7-15 and instead more enriched in F16-24 (Figure 1D-E), in accordance with our recently published work (Tkach et al., 2022). This observation suggests that 14-3-3 is not a reliable EV marker, but instead a marker of non-EV co-isolated contaminants. Finally, SEC fractions from two additional biological replicates of Nluc-CD63 or Nluc-CD9 conditioned media, pooled according to manufacturer’s instructions (i.e., F7-11 = EV fractions, F12-24 = non-EV fractions) were analysed by Transmission Electron Microscopy (TEM) (Figure 1F-G) and for Nluc activity and particle number (Figure S1D). We confirmed that the majority of CD63- or CD9-positive EVs from Nluc-CD63 and Nluc-CD9 cells, respectively, were detected in F7-11 (Figure 1F-G, Figure S1D), which contained at least 50% of total Nluc activity (Figure S1D).

Overall, we found that the majority of extracellular Nluc activity measured in Nluc-CD63 and Nluc-CD9 supernatants is associated to EVs, only less than 30% having a different origin (e.g., free proteins or small membrane fragments). Consequently, we concluded that measuring extracellular Nluc activity is a consistent and easy read-out of EV secretion compatible with high throughput screening procedures.

## 2.2 | Validation of the read-out for HCS screening by controlled manipulation of Nluc-CD63 and Nluc-CD9 secreting cells

Although validated in normal culture conditions, the use of our assay for screening a drug library brings additional constraints. One of the most obvious is the potential impact of some compounds of the drug library on cell viability, which would artificially increase Nluc release independently of EV secretion. Indeed, the MISEV2018 guidelines recommend to systematically report the level of cell viability in cultured cells producing EVs, since cell death may lead to release of both soluble and membrane bound structures such as apoptotic bodies (Théry et al., 2018). Therefore, to investigate how cell death resulting from compound toxicity affects the measurement of Nluc activity in the supernatant, we treated Nluc-CD63 and Nluc-CD9 cells with Puromycin. Increasing doses of Puromycin led to a parallel increase of Nluc activity in the supernatant of both cell lines (Figure S2A-B) and decrease of cell viability (quantified as number of Hoechst-labelled nuclei of the same cells, with dead cells characterized by round and bright nuclei). Thus, to avoid possible misinterpretations of our assay, we established a threshold of “acceptable” cell viability as around 85% of live cells, which increased extracellular Nluc activity by less than 30% (Figure S2A-B). To further challenge our assay, we measured Nluc activity in the conditioned medium of Nluc-CD63 and Nluc-CD9 cells treated with Bafilomycin A1, a drug known to increase exosome secretion (Cashikar & Hanson, 2019; Edgar et al., 2016; Eitan et al., 2016). As expected, Bafilomycin A1 treatment increased Nluc activity only in the supernatant of Nluc-CD63 cells (1.78 fold) but not in that of Nluc-CD9 cells (Figure S2C-D). Importantly, cell viability was not affected by this drug (Figure S2C-D).

This result shows that our assay is sensitive enough to reveal an increase of EV release regardless of any cell death event. Moreover, it allows addressing the specificity of the effect towards distinct EV populations (CD63- and CD9-positive, respectively).

## 2.3 | Identification of a drug increasing Nluc activity in the supernatant of Nluc-CD63 and Nluc-CD9 cells

With the established threshold to exclude effects of drug toxicity on Nluc activity, we next proceeded with the screening assay depicted in Figure 2A to identify compounds able to affect the secretion of Nluc-CD63 EVs, Nluc-CD9 EVs, or both. We exposed Nluc-CD63 or Nluc-CD9 cells to a library of 1,280 FDA- and EMA-approved compounds (V3, Prestwick) at 10  $\mu$ M final concentration. We simultaneously measured Nluc activity in the cell supernatant, and cell viability by labelling the nuclei of the secreting cells with Hoechst (dead cell nuclei highlighted with red arrowheads in Figure 2B), in order to monitor the toxicity of the administered compounds. The screening was performed twice independently and for each drug, the level of extracellular Nluc activity

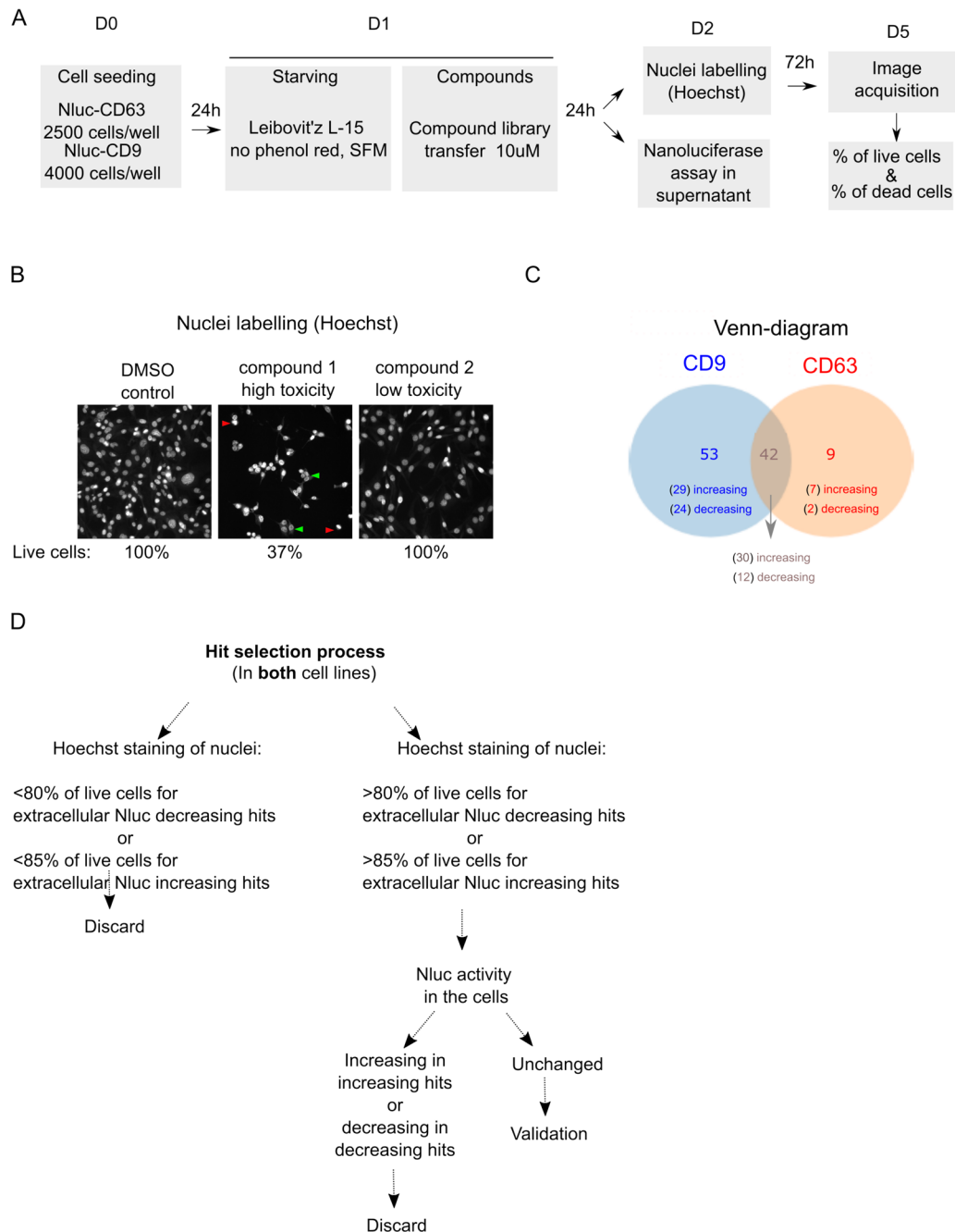


**FIGURE 2** Pipeline for high-content screen to identify drugs modulating extracellular Nluc activity in Nluc-CD63 and Nluc-CD9 cells. (A) Representative scheme of the screening protocol. SFM = serum-free medium. All drugs were used at 10  $\mu$ M. (B) Representative example images of Hoechst nuclei staining for DMSO negative control (100% live cells), a high toxicity compound (= compound 1: 37% live cells) or a low toxicity compound (= compound 2: 100% live cells). Very round and bright nuclei are specific of dead cells. Total number of nuclei (i.e., total number of live + dead cells) and number of dead cell nuclei are counted, to calculate the actual number of live cells, in each condition as compared to the DMSO control. Green arrowheads: live cells; red arrowheads: dead cells. (C) Venn-diagram summarizing the obtained screening results for two independent experiments. A total of 104 candidate compounds were identified. Among these, 53 only affected Nluc-CD9, nine only affected Nluc-CD63 and 42 affected both cell lines. For each group, the number of increasing or decreasing candidate compounds is reported. (D) Scheme of the decision-tree for candidate compounds selection process. Compounds resulting in less than 80% viability and decreasing extracellular Nluc or less than 85% viability and increasing extracellular Nluc in the screening step were discarded. In the secondary selection step, compounds inducing the same trend of effect extracellularly and intracellularly were discarded

was normalized by that of cells treated with DMSO as internal reference control. We expressed normalized extracellular Nluc activity as “Robust Z-score” (RZ-score, as described in materials and methods) and compounds qualifying as “outliers” in this statistical analysis, that is, candidates for modulating EV secretion, were defined by a RZ-score  $> 2$  or  $< -2$  (Table S1). We thus identified nine candidate compounds affecting Nluc-CD63, 53 candidate compounds affecting Nluc-CD9 and 42 candidate compounds affecting both (Figure 2C, Figure S2E, Table S1). We then applied the cell death threshold criteria described in Figure 2D, discarding 79 drugs resulting in less than 80–85% of cell viability (Tables S1 and S2). We selected 25 among the 104 total candidate compounds identified in the screening (see graphs in blue in Figure 3A and B) for which we secondarily measured the effect on intracellular Nluc activity (see graphs in red in Figure 3A and B). As we were seeking for drugs affecting specifically the release of EV-associated Nluc and not expression of the Nluc-fused molecules nor Nluc enzymatic activity, we discarded all the compounds that modulated in a similar way Nluc activity in the supernatant and intracellular Nluc activity (arrows in Figure 3A–B). Thus, we selected a group of four compounds modulating EV secretion: two that decreased (Dipivefrin hydrochloride, Metaraminol bitartrate) versus two that increased (Liothyronine, Homosalate) EV secretion in at least one of the two cell lines. We then re-validated them in both cell lines for intracellular and supernatant Nluc activity (Figure 3C–D). Homosalate induced a strong 3-fold (Nluc-CD63 cells) or 1.5-fold increase (Nluc-CD9 cells) of Nluc activity in the supernatant (blue graphs, Figure 3C–D), which was statistically significant ( $P = 0.02$ ). By contrast, the increase (Liothyronine) or decrease (Dipivefrin Hydrochloride or Metaraminol bitartrate) of Nluc activity observed with the other three drugs were relatively mild ( $\pm 20\%$ ) and not statistically significant. Thus we focused on Homosalate for further validation.

## 2.4 | Homosalate increases EV secretion enriching a population of SLC3A2/CD98-positive EVs

To confirm the effect of Homosalate using classical EV isolation and characterization methods, we treated MDA-MB-231 parental cells with Homosalate and isolated EVs using SEC. We confirmed the absence of detrimental effect of Homosalate on cell viability by Trypan Blue staining (Figure 4A). Strikingly, we observed that compared to control (DMSO) condition, Homosalate treatment induced a significant increase in particle number by NTA both in the total cell supernatant (input) and the EV-rich F7-11 fractions (Figure 4B), and in the number of CD63+ and CD9+ particles per field on TEM grids loaded with EVs from the same number of cells (Figure 4C). We next analysed the expression of EV markers in isolated EVs (F7-11) by Western Blot with EV samples isolated from the same number of secreting cells (Figure 4D). We observed an increase of EV makers SLC3A2/CD98, CD63, Syntenin, CD9 and CD81 and total proteins in general whereas no major changes were observed in the total cell lysates (CL) (Figure 4D, Figure S3A–B). Although we interpret a priori the Homosalate-induced increased in EV recovery by an increase in secretion, a decreased re-uptake by the producing cells would result in the same global extracellular increase. To test this hypothesis, we quantified efficiency of Nluc-CD9 EV uptake by parental MDA-MB-231 cells in the presence of Homosalate. As shown in Figure S4A, DMSO- and Homosalate-exposed cells captured Nluc-EVs with the same efficacy. Taken together, these data show that Homosalate increases EV release from parental MDA-MB-231. Importantly, Homosalate also increased particle release in two other human tumour cell lines, HeLa and MCF7 with minimal impact on cell viability, and in another one, Jurkat, but with a significant toxicity that, for this cell line, could participate in the observed increased EV release (Figure S4B–C). In mouse cells, Homosalate increased EV release by a spontaneously immortalized fibroblast cell line Pfa1 (Seiler et al., 2008), and, although to a lower extent, by the mouse mammary carcinoma E0771 (Figure S4D–E). To determine whether, besides increasing the total amount of released EVs, Homosalate also affected their composition, we next analysed EV secreted by Homosalate-treated MDA-MB-231 parental cells by WB loading the same number of particles (Figure 4E, Figure S3C–D). We observed that SLC3A2/CD98 and to a minor extent CD9 were increased (Figure 4E, Figure S3C–D). These data suggested that Homosalate primarily increased a population of EVs enriched in SLC3A2/CD98 and CD9. Consistently, our group previously showed that SLC3A2/CD98 is present on distinct CD63- or CD9-positive EVs populations secreted by HeLa cells, and is particularly enriched in the latter under certain conditions (Mathieu et al., 2021). To characterize EV subpopulations secreted by MDA-MB-231, we performed an EV co-immunoprecipitation assay using anti-CD63- or anti-CD9-coated beads with SEC-isolated EVs (Figure S5A). SLC3A2/CD98 co-immunoprecipitated with both CD63 and CD9, but the percentage of SLC3A2/CD98 that co-immunoprecipitated was higher with CD9 (97%) than with CD63 (86%) (Figure S5A). Similarly, we observed that only 83% of CD9 co-immunoprecipitated with CD63 (Figure S5A). Finally, only 63% of CD63 co-immunoprecipitated with CD9 (Figure S5A). These findings suggest that MDA-MB-231 secrete heterogeneous subpopulations of EVs characterized by different combinations of CD63, CD9 and SLC3A2/CD98, with a predominant sub-population of EVs enriched in SLC3A2/CD98, CD9 and CD63 and two minor subpopulations enriched either in SLC3A2/CD98 and CD9 but not CD63, or in CD63 alone. Immunoprecipitation did not show major differences in Homosalate-EVs as compared to control EVs released by DMSO-treated cells (Figure S5B). Thus, to identify additional combinations of surface proteins on EVs released by MDA-MB-231, we next used a multiplexed assay, which relies on capture of EVs on 37 types of beads, each coated with a different antibody, plus two isotype control beads, followed by global EV detection with mixed antibodies against the tetraspanins CD9, CD63 and CD81 (Koliha et al., 2016) (Figure 4F, top panels). We further customized this assay to label SLC3A2/CD98 on EVs after capture by the beads (Figure 4F, bottom panels). In control conditions (DMSO), we observed that EVs from MDA-MB-231 detected with both tetraspanins and SLC3A2/CD98

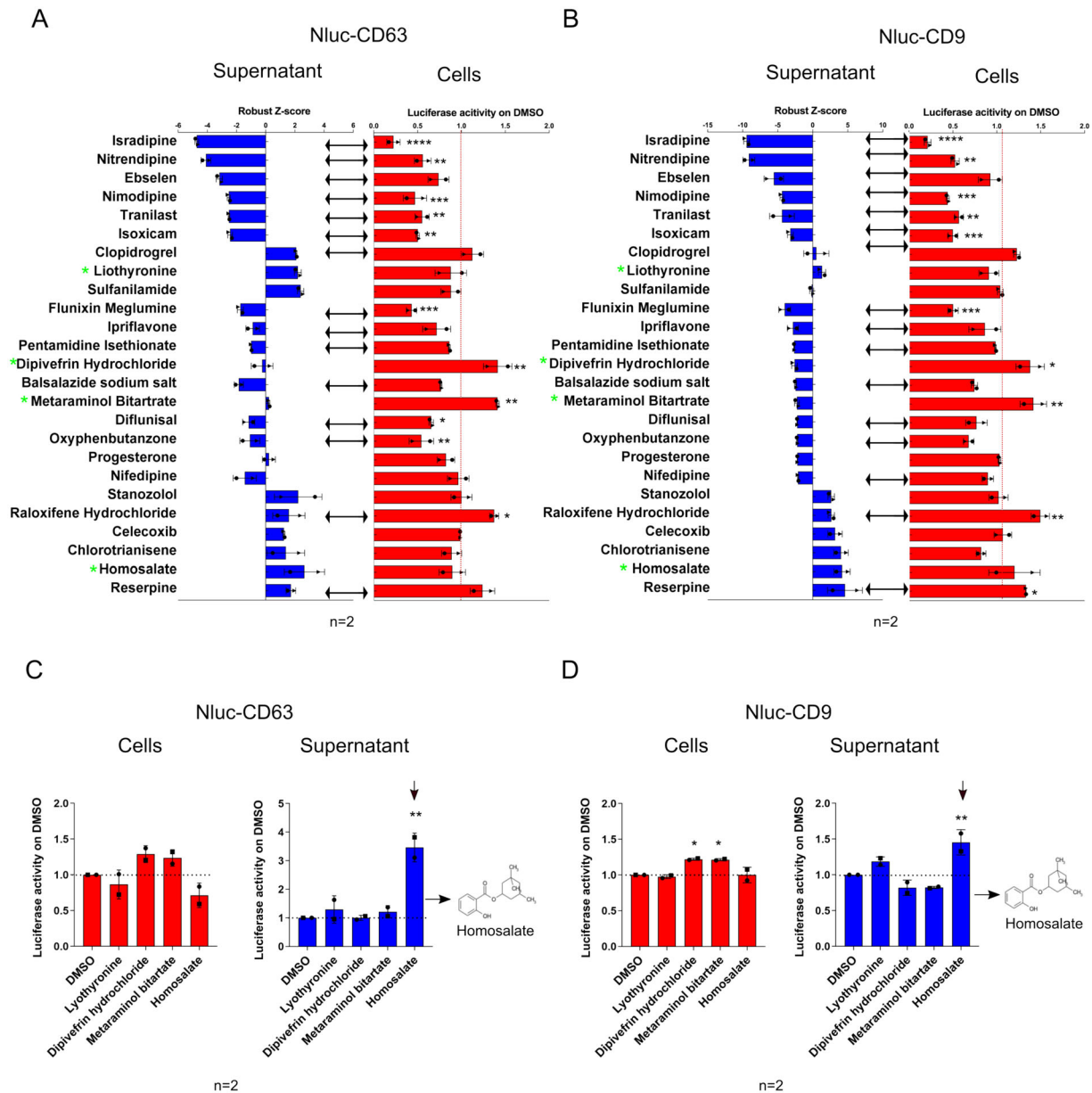


**FIGURE 3** Identification of a drug increasing extracellular Nluc activity in Nluc-CD63 and Nluc-CD9 cells. (A) and (B) Selection of 25 compounds from the 104 total candidates in Nluc-CD63 (A) and Nluc-CD9 (B) following criteria described in Figure 2D. Blue graphs: for each compound, extracellular Nluc activity intensity measured in the screening is reported as robust Z-score =  $[(\text{compound value} - \text{median of (Ref pop)}) / (\text{MADnc} \times 1.4826)]$ ,  $\text{MAD} = [\text{median} (|\text{Ref pop} - \text{median (Ref pop)}|)]$ . Increasing or decreasing hits were called according to the Threshold:  $|\text{Robust Z score}| > 2$  or  $< -2$ . Red graphs: for each compound, intracellular Nluc activity intensity upon treatment with  $10 \mu\text{M}$  of the candidate compounds was measured and reported as ratio on DMSO negative control. Data from two independent experiments are shown. Ordinary one-way ANOVA, multiple comparisons test and Dunnett's test:  $*P < 0.05$ ,  $**P < 0.01$ ,  $***P < 0.001$ ,  $****P < 0.0001$ . Arrows between blue and red show non-selected compounds inducing the same trend of effect in cells and supernatants in both independent experiments, whereas green \* symbols indicate compounds selected for further validation. (C) and (D) Validation of four of the identified candidates. For Nluc-CD63 and Nluc-CD9 cells, intracellular (red) versus supernatant (blue) Nluc activity was measured after treatment with Lyothyronine, Dipivefrin Hydrochloride, Metaraminol Bitartrate and Homosalate ( $10 \mu\text{M}$  each). Data are expressed as ratio on DMSO negative control and are from two independent experiments. Ordinary one-way ANOVA, multiple comparisons test:  $*P < 0.05$ ,  $**P < 0.01$

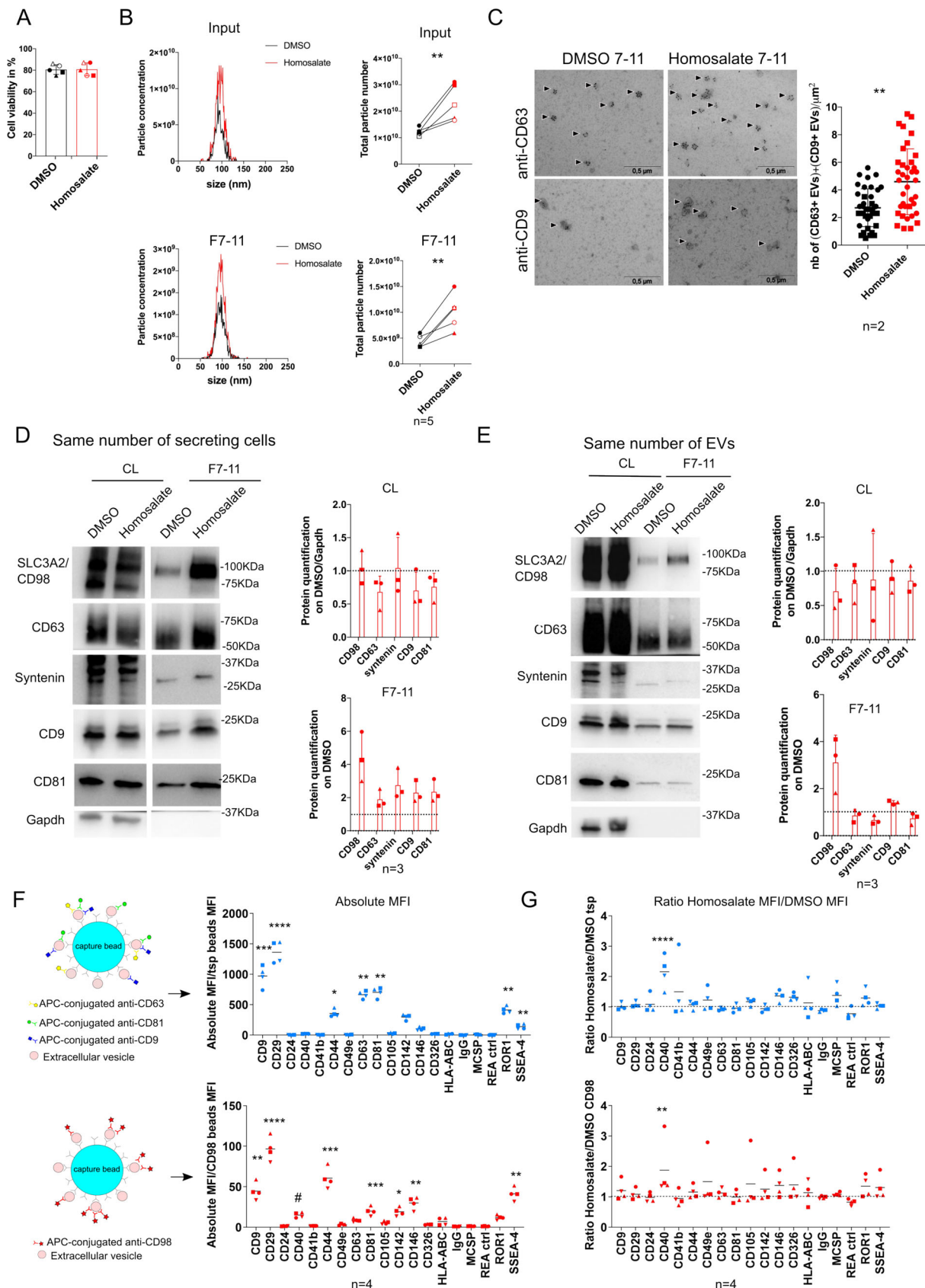


**FIGURE 4** Homosalate increases EV secretion enriching a population of SLC3A2/CD98-positive EVs. (A) Quantification of cell viability after Homosalate (10  $\mu\text{M}$ ) treatment in MDA-MB-231 parental cells. DMSO or Homosalate treated cells were counted after collection of conditioned media, using Trypan Blue as a reporter of cell death. Cell viability is expressed in percentage. Data from five independent experiments are shown. (B) Quantification of EVs induced by treatment with Homosalate. Left panel: one representative graph showing particle concentration/ $\text{cm}^3$  versus particle size measured by NTA in

(Continues)

**FIGURE 4** (Continued)

inputs (total conditioned medium) and F7-II (EV-rich SEC fractions) from  $27 \times 10^6$  DMSO or Homosalate treated cells. Right panel: Graphs show total particle number secreted from  $27 \times 10^6$  cells measured by NTA in DMSO or Homosalate treated cells for inputs and SEC F7-II, from five independent experiments. Paired parametric t-test:  $**P < 0.01$ . (C) Representative TEM images showing (CD63+) or (CD9+) EVs in F7-II released by  $2.7 \times 10^6$  DMSO or Homosalate treated cells. Arrowheads indicate EVs positive for CD63 staining (above) or CD9 staining (below). Graphs show quantification of the number (= nb) of (CD63+EVs) + (CD9+ EVs) per  $\mu\text{m}^2$ . Scale bar  $0.5 \mu\text{m}$ . Data from two independent experiments are shown, each dot represents EVs counted in one field (DMSO: 20 dots for replicate 1, 18 dots for replicate 2; Homosalate: 20 dots for replicate 1, 18 dots for replicate 2). Mann-Whitney test:  $**P < 0.01$ . (D) Western Blot analysis of markers SLC3A2/CD98, CD63, Syntenin, CD81 and CD9 in EVs released by cells treated with DMSO or Homosalate. Gels were loaded with EVs from the same number of secreting cells. Gapdh was used as normalizer for cell lysates (CL). CL from the equivalent of 200,000 cells were loaded, F7-II from the equivalent of  $2.7 \times 10^6$  secreting cells were loaded. Graphs show protein signal quantifications normalized first on Gapdh and then on DMSO for CL or normalized on DMSO for F7-II. Data from three independent experiments are shown. (E) Western Blot analysis of markers SLC3A2/CD98, CD63, Syntenin, CD81 and CD9 in EVs released by cells treated with DMSO or Homosalate, after gel loading with same numbers of particles. Gapdh was used as normalizer for CL. CL from the equivalent of 200,000 cells or an amount corresponding to  $4 \times 10^8$  particles for F7-II were loaded. Graphs show protein signal quantifications normalized first on Gapdh and then on DMSO for CL or normalized on DMSO for F7-II. Data from three independent experiments are shown. (F) Scheme of the multiplexed analysis strategy, and use on  $1.7 \times 10^9$  EVs from DMSO-treated MDA-MB-231 cells. Out of the 37 antibody-coated beads, only 17 leading to specific MFI (= MFI (beads+EVs) > MFI (beads-no EVs)) after staining with mixed anti-CD9/CD63/CD81 (top panel) or SLC3A2/CD98 are shown (bottom panel). Results obtained from four independent EV preparations are shown as individual dots. Kruskal-Wallis followed by Dunn's post-test comparing each capture bead with its correspondent isotype control. CD41b, CD81, CD105, HLA-ABC, SSEA-4 were compared to REA control and the rest were compared to IgG control:  $*P < 0.05$ ,  $**P < 0.01$ ,  $***P < 0.001$ ,  $****P < 0.0001$ ,  $\#P = 0.07$ . (G) The same multiplexed analysis was performed on  $1.7 \times 10^9$  EVs from Homosalate-treated MDA-MB-231. Ratio of specific MFI of Homosalate-EVs/DMSO-EVs after staining with anti-tetraspanins (tsp, top) or anti-SLC3A2/CD98. Results obtained from four independent EV preparations are shown as individual dots. Two-way ANOVA followed by Sidak's post-test comparing DMSO with Homosalate:  $**P < 0.01$ ,  $****P < 0.0001$

antibodies contained CD9, CD29, CD44, CD63, CD81 and SSEA-4. The SLC3A2/CD98 signal was specifically detected on EVs bearing CD142, CD146 or CD40 ( $P = 0.07$ ), whereas the tetraspanin signal was detected on EVs bearing ROR1 (Figure 4F). This observation suggests that SLC3A2/CD98-bearing EVs are enriched in specific surface markers including CD142, CD146 and CD40. We next compared EVs from Homosalate- and DMSO-treated cells. Subpopulations of EVs bearing CD40 with either tetraspanins or SLC3A2/CD98 were the most clearly upregulated upon Homosalate treatment (Figure 4G), suggesting that this combination of surface markers defines the EV subtype most prominently released upon Homosalate exposure. Taken together, these data indicate that Homosalate not only induces a sustained release of bulk EVs (Figure 4B-D), but also selectively increases some subpopulations of EVs.

## 2.5 | Homosalate and Bafilomycin A1 induce the release of EV subpopulations generated in distinct subcellular compartments

Bafilomycin A1 is a known specific increaser of release of exosomes (Bowman et al., 1988; Edgar et al., 2016; Eitan et al., 2016). We asked whether Homosalate showed the same specificity by comparing the effects of the two drugs. As expected, neither Homosalate nor Bafilomycin A1 increased cell death in parental MDA-MB-231 (Figure 5A) and both increased the number of particles by NTA (Figure 5B). This increase was due to increased EV release, and not to decreased EV re-uptake, since Nluc-CD9 EV uptake by recipient MDA-MB-231 cells in the presence of Bafilomycin A1 was similar (at 2 h) or even increased (at 16h) compared to the other conditions, possibly due to the inhibition of lysosomal degradation (Figure S4A). Then, we analysed the expression of EV markers by Western Blot normalized by same number of particles and observed that Homosalate reproducibly increased the release in EVs of SLC3A2/CD98 (in 4/5 biological replicates,  $P = 0.08$ ) (Figure 5C). Conversely, Bafilomycin A1 increased release in EVs of CD63 in 4/5 replicates ( $P = 0.09$ ) and of Lamp1 (a marker of late endosomal/lysosomal compartments (Carlsson, Roth, Piller, & Fukuda, 1988)) in 5/5 replicates ( $P = 0.006$ ), consistent with previous observations of a specific effect of this drug on exosomal EVs originating from late endosomes (Cashikar & Hanson, 2019; Edgar et al., 2016; Mathieu et al., 2021). Thus, the preferential increase of CD63 and Lamp-1 after Bafilomycin A1, and of SLC3A2/CD98 after Homosalate treatment suggests that the two drugs are acting on distinct subcellular compartments. To better define the subcellular origin of EVs induced by Homosalate or Bafilomycin A1, we analysed the intracellular localization of CD63, CD9 and SLC3A2/CD98 markers by immunofluorescence. As shown previously for HeLa cells (Mathieu et al., 2021), we observed that CD63 was localized mostly in intracellular compartments in DMSO-treated negative control, whereas CD9 was mainly localized at the plasma membrane and in few intracellular compartments (Figure S1C, Figure 5D, left panel). Interestingly, SLC3A2/CD98 co-localized with CD9. After treatment with Bafilomycin A1 we found an increased number of large CD63-positive perinuclear compartments, and CD9 and SLC3A2/CD98 appeared to accumulated more intracellularly (Figure 5D, right panel). By contrast, none of the analysed markers were accumulated intracellularly after Homosalate treatment and instead, SLC3A2/CD98 and CD9, but not CD63, were enriched at the plasma membrane (Figure 5D, middle panel). Co-localization measurements of these markers revealed that the amount of SLC3A2/CD98 co-localizing with CD9 in the DMSO control was around 80%, higher than the one co-localizing with CD63 (around 50%) (Figure 5E). This observation corroborates the data shown in Figure S5A, in which SLC3A2/CD98 preferentially

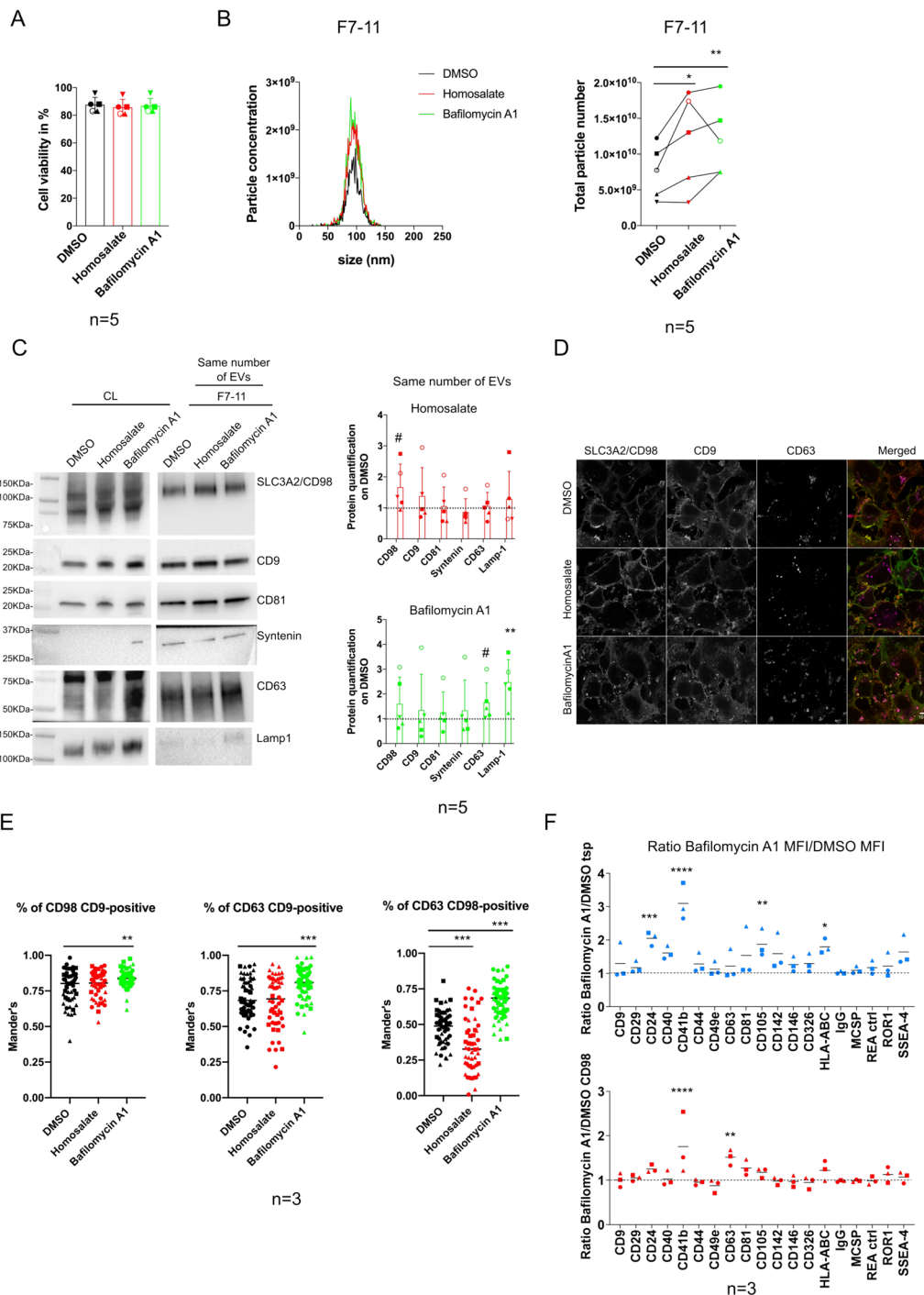


**FIGURE 5 Homosalate increases the secretion of plasma membrane derived EVs.** (A) Quantification of cell viability after Homosalate (10  $\mu$ M) and Bafilomycin A1 (100 nM) treatment in MDA-MB-231 parental cells. DMSO, Homosalate or Bafilomycin A1 treated cells were counted after conditioned media collection, using Trypan Blue as a reporter of cell death. Cell viability is expressed in percentage. Data from five independent experiments are shown. (B) Quantification of EVs induced by treatment with Homosalate and Bafilomycin A1 in MDA-MB-231 parental cells. Left panel: Graphs show particle concentration/cm<sup>3</sup> versus particle size measured by NTA in F7-11 (EV-rich SEC fractions) from 50  $\times$  10<sup>6</sup> DMSO, Homosalate or Bafilomycin A1 treated cells. Right panel: Graphs show total particle number secreted from 50  $\times$  10<sup>6</sup> cells measured by NTA in DMSO, Homosalate or Bafilomycin A1 treated cells for SEC F7-11. Data from five independent experiments are shown. Paired parametric t-test  $P = 0.04$ ;  $P = 0.002$ . (C) Western Blot analysis of EV markers SLC3A2/CD98, CD9, CD81, Syntenin, CD63 and Lamp-1 released after treatment with DMSO, Homosalate or Bafilomycin A1 after gel loading with same number of particles. CL from the equivalent of 200,000 cells or an amount corresponding to 4  $\times$  10<sup>8</sup> particles from F7-11 were loaded. Graphs show protein signal quantifications normalized to DMSO for F7-11 after treatment with Homosalate (above) or Bafilomycin A1 (below). Data from five independent experiments are shown. Unpaired, multiple t-test: # $P = 0.08$  (SLC3A2/CD98 in protein signal quantification after Homosalate treatment, top), # $P = 0.09$  (CD63 in protein signal quantification after Bafilomycin A1 treatment, bottom), \*\* $P < 0.01$ ). (D) Immunofluorescence of SLC3A2/CD98, CD63 and CD9 in

(Continues)

**FIGURE 5** (Continued)

MDA-MB-231 treated with DMSO, Homosalate or Bafilomycin A1. Scale bar: 10  $\mu\text{m}$ . (E) Graphs show Mander's correlation coefficients for CD98-CD9, CD63-CD9 or CD63-CD98 co-localization expressed as percentage. Ordinary one way Anova, multiple comparison test:  $**P < 0.01$ ,  $***P < 0.001$ . Data from three independent experiments are shown, each dot represents one counted cell (DMSO: 25 dots for replicate 1, 10 dots for replicate 2, 19 dots for replicate 3; Homosalate: 25 dots for replicate 1, 12 dots for replicate 2, 21 dots for replicate 3; Bafilomycin A1: 21 dots for replicate 1, 16 dots for replicate 2, 22 dots for replicate 3). (F) The same multiplexed analysis as in Figure 4(F-G) was performed on  $0.85\text{-}1.7 \times 10^9$  EVs from DMSO- or Bafilomycin A1-treated MDA-MB-231. Ratio of specific MFI of BafA1-EVs/DMSO-EVs after staining with anti-tetraspanins (tsp, top) or anti-SLC3A2/CD98 (CD98, bottom). Results obtained from three independent EV preparations are shown as individual dots. Two-way ANOVA followed by Sidak's post-test comparing DMSO with BafA1:  $*P < 0.05$ ,  $**P < 0.01$ ,  $***P < 0.001$ ,  $****P < 0.0001$

co-immunoprecipitated with CD9 than with CD63. Co-localization of CD63 and CD9 was also significant (70%). Homosalate did not change the amount of SLC3A2/CD98 nor of CD63 co-localizing with CD9 (Figure 5E), whereas Bafilomycin A1 increased both to, respectively, 85% and 80% (Figure 5D). By contrast, Homosalate treatment reduced the amount of SLC3A2/CD98 co-localizing with CD63 to 30%, whereas Bafilomycin A1 treatment increased it to 70%, indicating that this drug causes the two markers to be more accumulated in late endosomal compartments (Figure 5D). Biochemical changes of EV protein composition upon Bafilomycin A1 treatment were not clear upon immunoprecipitation (Figure S5C); however, Multiplexed bead-based analysis showed a few markers specifically upregulated on EVs released upon treatment by this drug, such as CD41b with both tetraspanins and SLC3A2/CD98, CD63 with SLC3A2/CD98 and CD24, CD105 and HLA-ABC with tetraspanins (Figure 5F).

Taken together, these data suggest that Homosalate and Bafilomycin A1 induce the release of distinct EV subpopulations. Bafilomycin A1 acts on EVs originating into intracellular, late endosomal compartments (= exosomes) enriched with CD63 and with an intracellular pool of SLC3A2/CD98 and CD9, whereas Homosalate mostly acts on a subpopulation of EVs enriched in SLC3A2/CD98 and/or CD9, which could rather originate directly at the PM (Figure 5D, middle panel) (= ectosomes) as previously described in HeLa (Mathieu et al., 2021).

## 2.6 | Homosalate-, but not Bafilomycin-derived EVs induce resistance to anchorage-loss and promote migration

Since Homosalate and Bafilomycin A1 induce the release of EVs derived from different subcellular compartments, we wondered whether Homosalate- and Bafilomycin A1-induced EVs could display different functional properties. Homosalate increases in vitro migratory and invasive properties of several breast cancer cell lines when administered at low concentrations ( $\geq 100$  nM) during several weeks (Alamer & Darbre, 2018) and is highly toxic at certain concentrations for luminal breast cancer MCF7 cells (Yazar & Kara Ertekin, 2020). Based on this knowledge, we wondered whether the EVs generated by MDA-MB-231 cells upon Homosalate treatment induced functional consequences when applied to recipient tumour cells. First, we administered  $5 \times 10^8$  of SEC-purified EVs (F7-11) from Homosalate- or Bafilomycin A1-treated MDA-MB-231 to MCF7 during 1 h and then we followed the behaviour of cells in real-time during 50h using the xCELLigence system to measure continuously adhesion and number of cells, as a proxy for cell growth. As shown in Figure 6A, the growth rate of MCF7 remained constant, in absence (= No EVs) or presence of either types of EVs.

We then reasoned that the migratory and invasive behaviour modulated by Homosalate could more rely on cell-cell or cell-ECM adhesion properties. Deprivation of extracellular matrix support can induce a particular type of anchorage-loss dependent cell death called "anoikis" (Frisch & Screaton, 2001). Both tumour and non-tumour cells of epithelial origin can resist to anoikis by enforcing cell-cell contacts and forming large cell aggregates (Kim et al., 2017; Zhang, Lu, Dazin, & Kapila, 2004) or can become more resistant to anoikis under certain conditions (Frisch & Francis, 1994). In several cases, resistance to anoikis has been considered as hallmark of increased tumour aggressiveness (Haemmerle et al., 2017; Paoli, Giannoni, & Chiarugi, 2013; Wang et al., 2018). To evaluate whether EVs could affect the capability of MCF7 to grow in absence of cell-matrix contacts, we fed MCF7 cells with a fixed number of EVs for 1 h, before subjecting them to an anoikis assay, in which cells are cultured for 24 h in the absence of cell-matrix contacts in ultralow-attachment plates (Frisch & Francis, 1994). Ability of cells to re-adhere and proliferate after exposure to anchorage-loss was followed in real time over 50 h by xCELLigence. MCF7 cells fed with EVs derived from Homosalate-treated cells recovered better than cells exposed to EVs from Bafilomycin A1-treated or control cells, or to no EVs at all (Figure 6B). Since anoikis is thought to involve cell death by apoptosis, we then asked if EVs could protect MCF7 cells from death induced by drugs. MCF7 cells fed by EVs for 1 h were subjected to a moderate dose of Staurosporine inducing 60% cell death (Figure S6A), and cell survival was measured at 24 h (Figure 6C, left panel). The three types of EVs had no effect on cell viability in these conditions. Caspase activity as a measure of ongoing apoptosis was clearly induced 6 h after exposure to a higher dose of Staurosporine (1  $\mu\text{M}$ ): here again, the three types of EVs neither increased nor decreased Caspase activity (Figure 6C, right panel). Of note, exposure to anchorage-loss did not result in bona fide apoptosis in MCF7 cells, neither at 6 h nor at 24 h, as measured by Caspase3/7 activity (Figure S6B-C). Strengthening cell-cell contacts is known to improve resistance to anoikis (Kim et al., 2017; Zhang et al., 2004). Since enhanced cell-cell contacts could also modify the ability of cells to migrate, we evaluated the

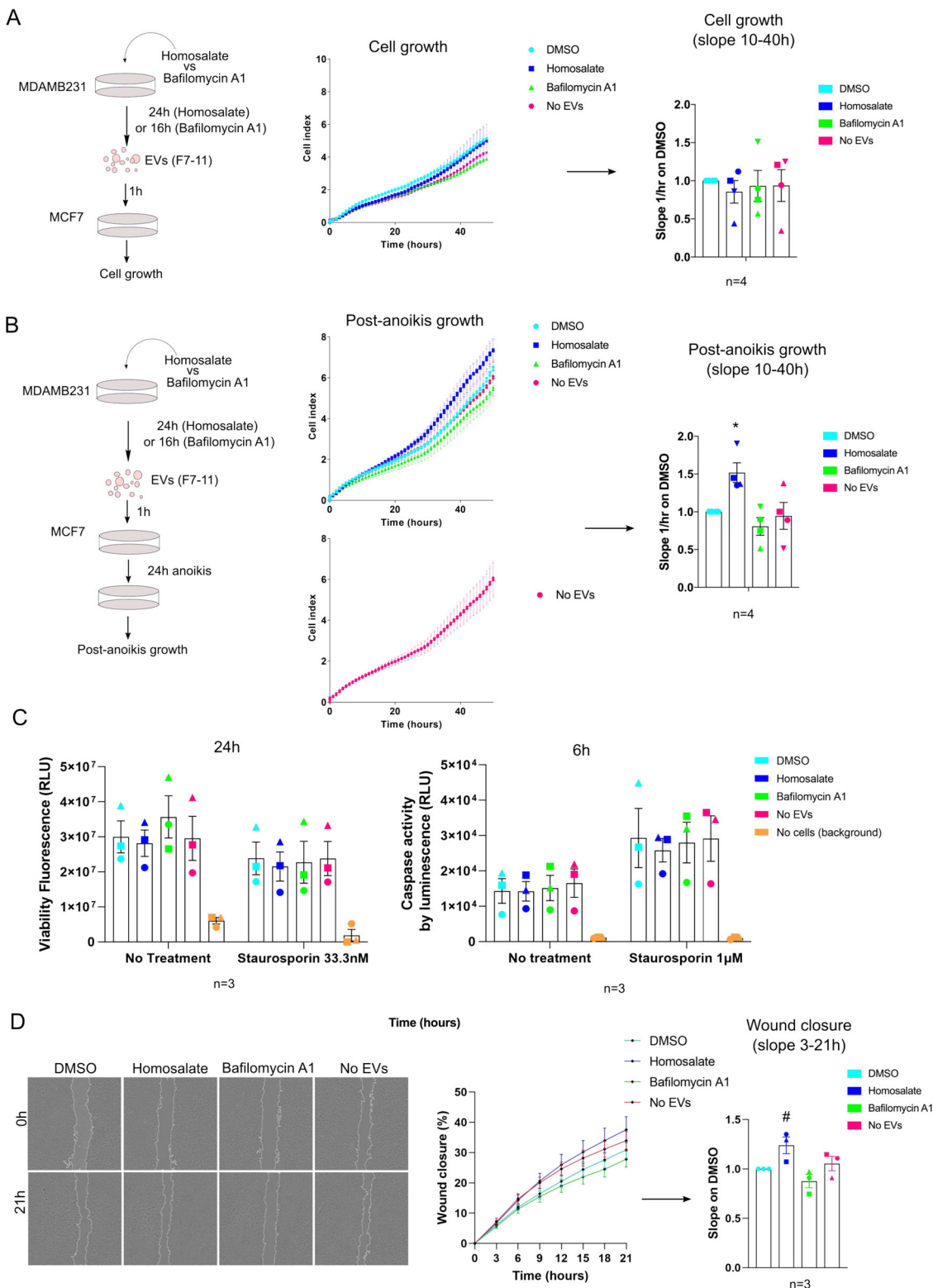


**FIGURE 6** Homosalate-, but not Bafilomycin A1-derived EVs induce resistance to anchorage-loss and increase migration. (A) Left panel: Representative scheme of EV treatment experiments in MCF7 cells. Middle panel: Representative graph of MCF7 real time adhesion and proliferation 1 h after treatment with EVs from DMSO, Homosalate (10 μM) or Bafilomycin A1 (100 nM) treated MDA-MB-231. Measurements were programmed every 30 min for a total time of 50 h in XCELLigence device. Right panel: graph showing quantification of slopes in the range 10–40 h. Data are expressed as ratio on DMSO negative control and are obtained from four independent experiments. Ordinary one-way Anova test non-significant (ns). (B) Left panel: Representative scheme of EV uptake followed by anoiikis/resistance to anchorage-loss assay in MCF7 cells. Middle panel: Representative graph of MCF7 real time adhesion and proliferation 1 h after uptake of EVs from DMSO, Homosalate or Bafilomycin A1 treated MDA-MB-231 and 24 h of anoiikis assay. Measurements were

(Continues)

**FIGURE 6** (Continued)

programmed every 30 min for a total time of 50 h in XCELLigence device. Right panel: graph showing quantification of slopes in the range 10–40 h. Data are expressed as ratio on DMSO negative control and are obtained from four independent experiments. Ordinary one-way ANOVA test:  $*P < 0.05$ . (C) Quantification of cell survival (fluorescence, left panel) and apoptosis (Caspase3/7 luminescence, right panel) in EV-treated MCF7, after exposure for, respectively, 24 h and 6 h, to, respectively, 33.3 nM and 1  $\mu$ M staurosporine. (D) Wound Healing assay: representative micrographs (left) and quantification of wound closure (right) by MCF7 cells pre-treated with EVs from DMSO, Homosalate- or Bafilomycin A1-treated MDA-MB-231 cells. Ordinary one-way ANOVA test:  $\#P = 0.07$

effect of EVs on cell migration in an in vitro wound healing assay (Figure 6D). In three independent biological replicates, MCF7 cells exposed to Homosalate-derived EVs closed the wound faster than cells exposed to DMSO- or Bafilomycin A1-induced EVs.

Taken together, these data indicate that EVs generated by MDA-MB-231 cells upon treatment with Homosalate are likely derived from PM and conferred to MCF7 cells enhanced capability to migrate and to grow in harsh conditions, that is, in the absence of a supportive extracellular matrix, which could increase their tumourigenic potential. Conversely, MVB-derived EVs induced by Bafilomycin A1 were not able to confer to MCF7 the same properties.

In conclusion, we show that specific drug treatments differentially affect not only the release and the composition of EVs but most importantly also their function.

### 3 | DISCUSSION

In the work presented here, we (1) established tools and a robotized process to quantify EVs bearing either one of two different markers, in a few microliters of cell conditioned medium, (2) successfully screened a bank of over 1,200 health agency-approved drugs for effect on EV release, (3) identified Homosalate as a potent drug increasing release of EVs likely originated from PM, and (4) showed that the Homosalate-induced EVs promote resistance to loss of attachment conditions, not observed with Bafilomycin A1-induced EVs.

In the literature, the number of chemical compounds affecting specifically release of given EV subtypes is still limited. For example, the drugs GW4869 (Trajkovic et al., 2008) or Manumycin A (Datta et al., 2017) have been proposed to decrease exosome release by ESCRT-independent or -dependent mechanisms, respectively. However, no direct proof was provided that these drugs did not affect the other EV types. A phospholipase D2 inhibitor, CAY10594, inhibits specifically secretion of Syntenin-containing exosomes formed by an ARF6-dependent pathway (Ghossoub et al., 2014), but ARF6 is also involved in ectosome release by other cells (Muralidharan-Chari et al., 2009). Recently, screening of a Syntenin-PDZ domain-focused fragment library led to the identification of a small molecule decreasing specifically the release of Syntenin-containing exosomes (Leblanc et al., 2020). The compound Y27632 decreases PM-derived ectosome release by targeting ROCK1 and ROCK2 kinases (Li, Antonyak, Zhang, & Cerione, 2012). Conversely, very few compounds have been shown to increase EV secretion. Bafilomycin A1 and other inhibitors of V-ATPase activity (Cashikar & Hanson, 2019) affect primarily exosome secretion. Ionomycin, which increases intracellular  $Ca^{2+}$  levels (Krämer-Albers et al., 2007), increases release of exosomes but also of other types of EVs, and can induce cell death. Therefore, identifying new drugs with different effects on EV subtypes and no side-effects such as death induction is still a desirable goal for the EV field.

Our study establish important factors to consider for HCS of drugs affecting EV release. We choose Nluc to establish a miniaturized and robotized process of EV quantification because this enzyme is small (19 kDa), has the minimum impact on the topology of tagged proteins, and is up to 100 folds more bright than other luciferase enzymes (e.g., Renilla or Firefly luciferases) (Hall et al., 2012). Nevertheless, Nluc is sensitive to the action of some chemical compounds which can inhibit its enzymatic activity (Auld & Inglese, 2004; Ho et al., 2013). Importantly, in our HCS of chemical compounds, we found several hits decreasing Nluc activity in the supernatant of cells (Figure 3A-B, Figure S2E). However, one of these candidate hits, Isradipine, had been described to inhibit Nluc enzymatic activity (Auld & Inglese, 2004), and like other compounds of the same family containing a phenyl-1,4-dihydropyridine core, Nitrendipine, Nimodipine or Nifedipine, they all inhibited Nluc activity in cells in our assay rather than inducing a decrease in EV release (Figure 3A-B). In addition to Nluc enzymatic activity itself, we also identified cell death as a critical parameter to be considered as it could increase leakage from the cell or the release of other membrane-bound structures (e.g., apoptotic bodies) (Théry et al., 2018) (Figure S2A-B). Finally, it should be mentioned that, because  $\sim 30\%$  of Nluc activity measured in the supernatant comes from elements other than EVs (e.g., free proteins, debris, etc.) (Figure 1B-C), drugs affecting release of EVs by less than 30% could not be reliably identified.

A low-throughput drug screening using Nluc activity as a read-out was previously successfully used (Cashikar & Hanson, 2019). The authors screened selected drugs and identified Bafilomycin A1 (and other compounds acting on V-ATPases) as increasers of Nluc-CD63 EV secretion (Cashikar & Hanson, 2019). We could confirm that Bafilomycin A1 increased extracellular Nluc activity in Nluc-CD63 but not Nluc-CD9 cells (Figure S2C-D), highlighting a differential effect of this MVB- modulating drug on CD63 or CD9 positive EV secretion. In another study, the use of a dual reporter system of CD63-Turbo-Luciferase-CD9-Emerald-Green allowed to identify several compounds regulating the secretion of CD63-CD9 double positive EVs by immune

cells (Shpigelman et al., 2021). Turbo-Luciferase could be particularly suitable for high-throughput screenings because it is less sensitive to chemical compound interference (Auld et al., 2018).

Our screening allowed the identification of Homosalate as robust increaser of EV secretion in MDA-MB-231 parental cells and in other tumour cell lines (Figure 4, Figure S4). The multiplexed analysis of surface markers on EVs showed that Homosalate increased the secretion of EVs bearing different combinations of markers as compared to EVs induced by Bafilomycin A1 (Figure 4G, 5F). The intracellular localization analyses confirmed previous findings from our group in HeLa cells, showing that SLC3A2/CD98 and CD9-positive EVs are mainly generated at the PM (= ectosomes), while CD63-positive EVs are mainly generated in MVBs (= exosomes) (Mathieu et al., 2021). Consistently, in our MDA-MB-231 cellular model in control conditions (= DMSO), CD63 was mainly localized in intracellular perinuclear compartments, whereas CD9 and SLC3A2/CD98 were more localized at the PM (Figure 5D), although neither of these markers were exclusively restricted to a single compartment (i.e., only PM or only MVB). Homosalate increased membrane staining of SLC3A2/CD98 and CD9, while Bafilomycin A1 increased the accumulation of CD63, CD9 and SLC3A2/CD98 in intracellular compartments (Figure 5D), and the release of EVs bearing simultaneously SLC3A2/CD98 and CD63 (Figure 5F). This suggests that Bafilomycin A1 acts on the intracellular pools of these proteins which will be subsequently co-expressed on secreted exosomes, as opposed to Homosalate which would act on the membrane pools of SLC3A2/CD98 and CD9 to give rise to ectosomes.

Homosalate was chosen because of its prominent effect on extracellular Nluc activity both in screening and in further validation steps. Other compounds also had relevant effects on EVs expressing CD63, CD9 or both. For example, even though their effect on extracellular Nluc activity was not as striking as that of Homosalate, Metaraminol Bitartrate or Dipivefrin Hydrochloride could be promising specific inhibitors of CD9-containing EVs release (Figure 3A–B, Table S1–S2), since they induced a consistent decrease of extracellular Nluc activity in screening and further validation steps. Regular EV quantification and characterization analyses are still needed to validate these drugs as novel EV inhibitors.

Homosalate is an anti-inflammatory drug commonly used as a chemical UV-screen in sun lotions (Couteau, Chauvet, Papis, & Coiffard, 2012; Wang, Marling, Plum, & Deluca, 2017). However, it displays estrogen-like properties and is suspected to be a potential endocrine disruptor dangerous for health (Krause et al., 2012). Here we identified an unsuspected action of Homosalate, that is, increasing EV release from different tumour cell lines. We demonstrated that in MDA-MB-231 triple negative breast cancer cells, EVs induced by Homosalate are generated in a distinct subcellular compartment compared to those induced by Bafilomycin A1. Not last, we demonstrated that EVs secreted by MDA-MB-231 upon treatment with Homosalate are endowed with a particular function: making other recipient tumour cell lines (i.e., MCF7 luminal breast cancer cells) more resistant to anchorage-loss. In general, primary epithelial cells are dependent on anchorage and cell-cell contacts, and resistance to loss of cell matrix contacts can be a hallmark of increased tumour aggressiveness (Haemmerle et al., 2017; Paoli et al., 2013; Wang et al., 2018), although it can be also a property of some non-tumour epithelial cells which develop it to accommodate regular trypsinization (Kim et al., 2017). MCF7 is relatively resistant to anoikis, as it does not undergo apoptosis upon low-attachment culture, (Figure S6B–C), therefore, we chose it as good versatile model to identify either protective or detrimental effects in this anoikis resistance assay. The safety of Homosalate in cosmetics is still a matter of debate (Opinion, 2020). Although our findings must be completed by additional studies on effective capacity of Homosalate to contribute to cancer progression, they could worsen the concern about using this compound in certain skin-care products.

## 4 | MATERIALS AND METHODS

We have submitted all relevant data of our experiments to the EV-TRACK knowledgebase (Van Deun et al., 2017), with the following accession number (EV-TRACK-ID: EV210281) .

### 4.1 | Cell culture and transfection

MDA-MB-231, MCF7, and HeLa were cultured in our laboratory for the last 20 years, after initial obtention from the American Type Culture collection (ATCC). They were validated by short tandem repeat (STR) sequencing in 2018. Jurkat E6-1 cells were obtained from the ATCC. Mouse Pfa1, MDA-MB-231, MCF7 and HeLa were cultured in Dulbecco's modified Eagle's medium (DMEM-Glutamax, Gibco), with 10% of Fetal Calf Serum (FCS, Gibco), 100U/ml penicillin and 100 µg/ml streptomycin (Gibco). Jurkat were cultured in Roswell Park Memorial Institute 1640 medium (RPMI-1640-Glutamax, Gibco), with 10% of Fetal Calf Serum (FCS, Gibco), 100U/ml penicillin and 100 µg/ml streptomycin (Gibco). E0771 were cultured in this same medium complemented with 10 mM HEPES and 50 µM β-mercaptoethanol. Cell lines were grown at 37°C, under 5% CO<sub>2</sub>, in humidified incubators and routinely tested using Myco detection Kit (Eurofins) for mycoplasma contamination. Only mycoplasma negative cells were used for experiments. MDA-MB-231 bulk or stable populations overexpressing Nluc-CD63 or Nluc-CD9 constructs were obtained using an electroporation-based transfection protocol optimized for this cell line (Amaxa Cell Line Nucleofector Kit V, Lonza). Briefly,  $1 \times 10^6$  cells were harvested by trypsinization and were mixed with 100 µl of room temperature

reconstituted Nucleofector solution combined with 2  $\mu\text{g}$  of the DNA construct of interest. The solution was transferred into a certified cuvette and cell electroporation was conducted using Nucleofector program X-013 (Amaxa Nucleofector, Lonza). Electroporated cells were immediately resuspended in pre-warmed phenol-free Leibovitz's L-15 medium (Fisher) with 10% of FCS and seeded in a 24 well plate. After 24 h, cells were harvested by trypsinization and resuspended in DMEM-Glutamax medium with 10% of FCS, 100 U/ml penicillin, 100  $\mu\text{g}/\text{ml}$  streptomycin and 2 mg/ml of geneticin as selection antibiotic. A portion of the resuspension volume corresponding to 1/3 was seeded in 10 cm dishes for low density culture to obtain clonal populations and a portion corresponding to 1/10 was seeded in a 24 well plate to obtain a bulk population. Clonal populations resistant to geneticin selection appeared after  $\sim 20$  days of culture and were collected manually using cloning discs (Scienceware cloning discs, Sigma-Aldrich). Collected clones were transferred in 96 well plates and once they reached confluence they were further selected by mean of Nluc activity measurement (Nano-Glo Luciferase Assay System, Promega, see details in sections below) in supernatants or in cells.

## 4.2 | Plasmids

Nluc sequence was PCR derived using the indicated primers (Forward: ATTACTACCGGTATGGTCTTCACACTCGAAGATTTTC; Reverse: ATTACTCTCGAGCGCCAGAATGCGTTCGCACAG) from a Nluc construct (kind gift of Michael Boutros). Nluc-CD63 construct was obtained by removing RFP sequence from RFP-CD63 (kind gift of Walther Mothes) using AgeI and XhoI restriction enzymes (New England Biolabs) and by replacing it with Nluc sequence using the same enzymes. Nluc-CD9 construct was obtained as follows: CD9 sequence was first PCR derived from tdTomato-CD9-10 construct (kind gift of Michael Davidson) using the indicated primers (Forward: CTCAAGCTTCCCCGGTCAAAGGAGGCA; Reverse: ATCCGCAGGAACCGCGAGATGGTCTAG). Then, a Renilla-luciferase-HSP70 construct previously obtained in our laboratory by removing GFP sequence from GFP-HSP70 construct (Addgene, #1525) with XhoI and SpeI restriction enzymes (New England Biolabs) was used as intermediate. Briefly, HSP70 sequence was removed from Renilla-luciferase-HSP70 and was replaced by CD9 sequence using XhoI and SpeI restriction enzymes. Finally, Renilla-luciferase sequence was removed using AgeI and XhoI restriction enzymes and was replaced by Nluc sequence using the same enzymes.

## 4.3 | Nanoluciferase detection assay

Nano-Glo Luciferase Assay System (Promega) was used to quantify Nluc activity both in cells and in supernatants of Nluc-CD63 and Nluc-CD9 cells. Experiments were conducted in 96 well plates (red graphs Figure 3A-B), 384 well plates (blue graphs Figure 3A-B, Figure S2) or 24 well plates (Figure 3C-D). First, cells were seeded in the various multi-well formats according to their different growth rates: 96 well plates: [16,000 Nluc-CD63 and 26,000 Nluc-CD9]; 384-well plates: [2,500 Nluc-CD63; 4,000 Nluc-CD9]; 24-well plates: [101,000 Nluc-CD63; 165,000 Nluc-CD9]. After 24 h, cells were washed 1 X with phenol free, serum free Leibovitz's L-15 medium and the same medium was added on cells (for 96-well plates: 100  $\mu\text{l}$ , for 384-well plates: 50  $\mu\text{l}$ , for 24-well plates: 500  $\mu\text{l}$ ). When required by the experiment (as for Figure 2-3 and Figure S2), drugs were added at this step to the phenol red free, serum free Leibovitz's L-15 incubated on cells (DMSO 0,1%, Bafilomycin A1 100 nM, Puromycin 1;1.5;2;3  $\mu\text{g}/\text{ml}$ ). To measure Nluc activity in the supernatant of cells, we proceeded as follows: to avoid to disturb adherent cells, only a fraction of cell conditioned medium was retrieved (for 96-well plates: 80  $\mu\text{l}$ , for 384-well plates: 40  $\mu\text{l}$  and for 24-well plates: 50  $\mu\text{l}$ ). Then, collected supernatants were centrifuged at 350 g for 10 min at RT to eliminate dead cells and debris. To prevent disruption of cell pellet, only a fraction of the resulting centrifuged supernatant (for 96 well plates: 60  $\mu\text{l}$ , for 384 well plates: 30  $\mu\text{l}$ , for 24 well plates: 40  $\mu\text{l}$ ) was collected and transferred to 96 well white plates (Corning #3912). For Nluc activity measurement, the reagent of Nano-Glo Luciferase Assay System was reconstituted according to manufacturer's instructions and was added to the supernatant at a 1:6 ratio. When performed, the measurement of intracellular Nluc activity was done as follows: cells were first washed 1X with phenol free, serum free Leibovitz's L-15 medium leaving a residual of 25  $\mu\text{l}$  of medium, and then Nano-Glo Luciferase Assay reagent was added at a 1:4 ratio. Luminescence activity was read using iD3 SpectraMax microplate reader (Molecular Devices, California, USA) or Centro LB 960 microplate luminometer (Berthold, Germany). For Nluc activity measurement during drug screening, a specific protocol is fully described in the section below.

## 4.4 | Screening of the drug library

### Cell seeding and library addition

Cells were amplified over a week before the screening step. For cell passages, cells were washed with phosphate buffered saline (PBS, Eurobio) and detached with Trypsin (Gibco Life Technologies #12605010) for 10 min at 37°C. The compound library was

purchased from Prestwick Chemicals V3 and corresponds to a unique collection of 1,280 off-patent small molecules, mostly approved drugs by FDA, EMA and other agencies. All chemical compounds were diluted in DMSO as 10 mM stock solution, and represent four 384-well plates. Cells were counted using T4 Cellometer (Nexcelom) and optimum cell densities were obtained as 2,500 cells/well and 4,000 cells/well for Nluc-CD63 and Nluc-CD9, respectively. The screening was performed at same early cell passages for both replicate experiments according to the optimized amount of cells seeded in 384-well plates (ViewPlate-384 Black Perkin Elmer, #6007460) using a Multidrop Combi (Thermo Fisher Scientific) in 40  $\mu$ l of total cell media.

Around 24 h after cell seeding, cell media was removed from the plates and cells were washed once with 40  $\mu$ l of phenol red free, serum free Leibovitz's L-15 medium. A total of 40  $\mu$ l of the same Leibovitz's L-15 medium was robotically added to the plates (MCA 384, Tecan). Briefly, 2  $\mu$ l/well of each compound at 2 mM were mixed in a pre-dilution plate containing 78  $\mu$ l/well of cell medium, and 10  $\mu$ l of this solution were dispensed into each well of a 384-cell plate, in order to obtain a final concentration of 10  $\mu$ M and 0,5% of DMSO. DMSO was present in columns 1, 2, 23 and 24, and represents internal plate solvent controls. The screening was performed in two biological replicates for both cell lines.

## Nluc assay and cell labelling

After 24 h, 40  $\mu$ l of medium were transferred from cell plates to V-shaped 384-well plates using the MCA-384 head. Plates were then centrifuged at 350 g for 10 min at RT. 30  $\mu$ l of centrifuged supernatant were then transferred to flat bottom plates with the MCA-384 head. Nanoluc reagent was freshly reconstituted according to manufacturer's instructions (Nano-Glo Luciferase Assay System, Promega). 5  $\mu$ l of reconstituted solution were added to each well using a MultiDrop Combi. Plates were shaken for 30 s at 300 rpm on an orbital shaker (Titramax 100, Heidolph) prior to reading. Luminescence was recorded using a CLARIOStar (BMG Labtech) (gain = 3,600). In the meantime, cells were processed for nuclei labelling performed as follows: cells were fixed in a 3% formaldehyde solution for 15 min using the MCA 384 followed by 1 h incubation with the dye Hoechst 33342 (1:500, Sigma, #14533). Then PBS solution was added on top of it. Plates were kept at 4°C for 72 h prior to image acquisition.

## Images acquisition and analysis

Image acquisition of Hoechst 33342 fluorescent nuclei (excitation: 361–497 nm; emission 460–490 nm) was performed using the INCell analyser 6500HS automated system (GE Healthcare, USA) at a 10X magnification (Nikon 10X/0.451, Plan Apo, CFI/60), using the same exposure time for all plates in the experiment and across replicate experiments. Plates were loaded onto the microscope system with Kinedx robotic arm (PAA, UK). 16-bit images of four different positions in each well were acquired. The total number of cells measured in a field was typically around 350. For the screen, a total of 3,072 (8  $\times$  384-well plates) wells were imaged, resulting in 12,288 grey scale images (3072  $\times$  4 fields of view) per replicate experiment. We then made use of morphological characteristics of Hoechst-labelled nuclei to distinguish dead cells (Crowley, Marfell, & Waterhouse, 2016) using INCell Analyser 3.7 Workstation software (GE Healthcare). Cells were classified as alive or dead and % of dead cells computed for each drug-treated and control DMSO wells.

## Data analysis and hit calling

Screening data quality was graphical reviewed as scatter plots and plate heat-maps to depict any bias or technical issues using in-house tools (Biophenics platform, Institut Curie). Raw luminescence signals and cell count were first log transformed before Tukey's two-way median polishing (Birmingham et al., 2009; Mosteller, 1977), then normalized as follows: sample median and median absolute deviation (MAD) were calculated from the population of each internal plate data points (named as Ref pop) and used to compute Robust Z-scores (RZ-scores, from (Iglewicz & Hoaglin, 1993)) according to the formula:  $RZ\text{-score} = [\text{compound value} - \text{median}(\text{Ref pop})] / [1.4826 \times \text{MAD}(\text{Ref pop})]$  where *compound value* corresponds to the drug-treated data point, where MAD is defined as the median of the absolute deviation from the median of the tested wells. This statistical analysis largely used in the high-throughput screening field incorporates information on sample variation and is based on median and median absolute deviation (MAD) which improves hit selection when compared to mean and standard deviation (SD)-based methods. R Z-score is indeed considered a robust method to improve hit selection as described by (Birmingham et al., 2009; Chung et al., 2008). Median polished cell count values were scaled as:  $\text{Proliferation} (\%) = 100 \times [\text{compound value}] / [\text{median}(\text{negative control})]$ . Hits were identified per replicate experiment as those compounds modulating EV secretion (threshold applied is:  $|RZ\text{-score}| > 2$ ), in two replicate experiments). Hit values were computed as median values in the final hit list. Selected compounds were subsequently annotated in regards to the Proliferation (%) and % Dead cells, in order to identify compounds which could affect cell viability.

## 4.5 | EV isolation and drug treatment

For EV isolation,  $6 \times 10^6$  of MDA-MB-231 parental cells were seeded per 15 cm culture dish in an optimized number of dishes to obtain  $70 \times 10^6$  (Figure 1),  $27 \times 10^6$  (Figure 4) or  $50 \times 10^6$  (Figure 5) secreting cells. After 24 h, cells were washed 1 X with PBS (Eurobio) and 15 ml of serum free, phenol red free Leibovitz's L-15 were added. For experiments in Figures 4 and 5 DMSO (0.1%), Homosalate (10  $\mu$ M) or Bafilomycin A1 (100 nM) were added to phenol-red free, serum-free Leibovitz's L-15 medium incubated on cells during 24 h (DMSO and Homosalate) or 16 h (Bafilomycin A1). The day after, cells were counted and the percentage of cell viability was determined using Trypan Blue (Invitrogen). Experiments were performed with cells showing  $\geq 75\%$  viability. In parallel, conditioned media were harvested and centrifuged at 300 g for 10 min at 4°C to remove dead cells and debris. Then, resulting supernatant was centrifuged at 2,000 g for 20 min at 4°C to discard large EVs in the 2K pellet and then concentrated on a sterilized Sartorius Centrifugal Filter (MWCO = 10 kDa; Sartorius, #VS2001) or Centricon Plus-70 Centrifugal Filter (MWCO = 10 kDa; Millipore, #UFC701008). Media concentrated to  $\sim 500 \mu$ l were overlaid on 35 nm qEV size-exclusion columns (Izon, SP5) for separation. According to manufacturer's instructions, SEC fractions were collected in 500  $\mu$ l volume. For experiments in Figure 1B and C, we collected SEC fractions one by one from F1 to F24. Then, not concentrated SEC fractions were individually analysed in terms of particle number using Nanoparticle Tracking Analysis (NTA) (Particle Metrix ZetaView), protein concentration using BCA (Pierce BCA Protein Assay Kit, Thermo Scientific) or Nluc activity using Nano-Glo Luciferase Assay System (Promega). When comparing drug-treated versus DMSO negative control cells (Figures 4 and 5), concentrated conditioned media from same number of secreting cells were used for SEC. In this case, SEC fractions collected in 500  $\mu$ l volume were pooled as F7-11 (EV-rich = 2.5 ml) or as F12-24 (protein-rich = 6.5 ml). Pooled fractions were further concentrated using 10 kDa cut-off filters (Amicon Ultra-15, Millipore) before NTA, Western Blot or Transmission Electron Microscopy (TEM). To compare the effect of drug treatments on particle secretion from different tumour cell lines (MCF7, HeLa, Jurkat, Pfa1, E0771, Figure SF4) we adopted a procedure similar to what was described before, except that  $2.2 \times 10^6$  (HeLa, Pfa1, E0771),  $4.4 \times 10^6$  (MCF7) cells were seeded into 10 cm cell culture dishes or  $10 \times 10^6$  in T25 flasks (Jurkat). Drugs were added in serum free DMEM or RPMI (Jurkat). Particle number from same number of secreting cells was then measured by NTA directly in conditioned media after 300 g followed by 2,000 g centrifugations and concentration using sterilized Sartorius Centrifugal Filter (MWCO = 10 kDa; Sartorius, #VS2001).

## 4.6 | Nanoparticle tracking analysis (NTA)

NTA was performed using ZetaView PMX-120 (Particle Metrix) equipped with a 488 nm laser, at 10X magnification, with software version 8.05.02. The instrument settings were 22°C, gain of 26 and shutter of 70. Measurements were done at 11 different positions (two cycles per position) and frame rate of 30 frames per second. Image evaluation was done on particles with Minimum Brightness: 20, Minimum Area: 10, Maximum Area: 500, Maximum Brightness: 255. Tracking Radius2 was 100, Minimum Tracelength: 7.

## 4.7 | Western blot

Cell lysates (CL) for Western Blot were obtained by incubating  $1 \times 10^6$  cells in 25  $\mu$ l of lysis buffer (50 mM Tris, pH 7.5, 0.15 M NaCl, 1% Triton X-100) with 2% complete protease inhibitor (Roche) for 15 min on ice, followed by a 13,000 rpm centrifugation for 20 min at 4°C to recover the supernatant. The amount of CL used for Western Blot was the equivalent of 200,000 cells. For EVs isolated in F7-11, the amount used for Western Blot was adjusted either by same number of secreting cells (Figure 4D:  $2.7 \times 10^6$ ) or by same number of particles (Figure 4E, Figure 5C:  $4 \times 10^8$  measured in NTA). For EVs isolated in singularly collected fractions, the used amount corresponded to 25  $\mu$ l of the 500  $\mu$ l of each not-concentrated fraction from  $70 \times 10^6$  secreting cells. Samples were mixed with Laemmli sample buffer (BioRad) without  $\beta$ -mercapto-ethanol. After boiling 5 min at 95°C, samples were loaded on a 4–15% Mini-protean TGX-stain free gels (BioRad). Transfer was performed on Immuno-Blot PVDF membranes (BioRad), with the Trans-blot turbo transfer system (BioRad) during 7 min. Blocking was performed during 30 min with Roche blocking solution in TBS 0.1% Tween. Primary antibodies were incubated overnight at 4°C and secondary antibodies during 1h at room temperature (RT). Development was performed using Clarity western ECL substrate (BioRad) and the ChemiDoc Touch Imaging System (BioRad). Membranes were incubated with the following antibodies: mouse anti-human SLC3A2/CD98 1/3000 (clone 2B10F5 ProteinTech), mouse anti-human CD63 1/1000 (clone H5C6, BD Bioscience), mouse anti-human CD9 1/1000 (clone MM2/57, Millipore), mouse anti-human CD81 1/1000 (clone TS81, Diaclone), rabbit anti-human 14-3-3 1/1000 (EPR6380, GeneTex), rabbit anti-human Lamp1 1/1000 (clone EPR4204, GeneTex), mouse anti-Gapdh (clone 1E6D9, ProteinTech). Monoclonal rabbit anti-human Syntenin (used 1/1000) was a gift from P. Zimmermann. Secondary antibodies: HRP-conjugated goat anti-rabbit IgG (H+L) and HRP-conjugated goat anti-mouse IgG (H+L) were purchased from Jackson Immuno-Research.

## 4.8 | Immunofluorescence

The day before the treatment, 100,000 parental, Nluc-CD9- (clone 3) or Nluc-CD63-(clone 7) MDA-MB-231 cells were seeded on 12 mm diameter coverslips coated with polyornithine (15  $\mu\text{g}/\text{ml}$ ). For Figure 5D, parental cells were treated with 0.1% DMSO for 24h, 10  $\mu\text{M}$  Homosalate in 0.1% DMSO for 24h or 100 nM Bafilomycin A1 in 0.1% DMSO for 16h. After the treatments, they were fixed with 4% paraformaldehyde (PFA) (EMS) during 15 min at RT. The cells were incubated for 1h in a blocking solution: PBS containing 0.5% saponin and 0.1% BSA. Then primary and secondary antibodies were successively incubated during 1h each at RT in PBS containing 0.1% saponin and 0.1% BSA. Coverslips were then mounted on slides with Fluoromount G (Invitrogen). Images were acquired on a Zeiss LSM 780 confocal microscope using an alpha Plan-Apochromat 63x/1.46 Oil with the following acquisition parameters: average per line 2, pixel size depending on the sample between 81 and 106 nm, z-step 0.33  $\mu\text{m}$  for stack imaging. On each slide, laser powers were set to avoid saturation and allow subsequent quantification. At least two fields were captured to image a total of at least 10 cells per experiment (three independent experiments) with a minimum of 54 cells per drug treatment, or 75 cells for comparison of parental, Nluc-CD9 and Nluc-CD63 cells. Image analysis was performed with ImageJ. A median filter of 2-pixel radius was first applied to remove noise, then a subtract background with a 20 rolling radius was done. Then, to measure colocalisation between two channels, JACoP plug-in (Bolte & Cordelières, 2006) was used to calculate Mander's coefficients in each individual cell. Signal threshold Intensity to measure Mander's coefficients was calculated with the Otsu's method (Otsu, 1979). Coverslips were incubated with the following primary antibodies: SLC3A2/CD98 antibody (clone 590559 1/500, R&D Systems), mouse IgG2b anti-human CD63 (clone TS63b 1/100, available upon request to E. Rubinstein: [eric.rubinstein@inserm.fr](mailto:eric.rubinstein@inserm.fr)) and mouse IgG1 anti-human CD9 (clone TS9 1/100) (commercially available at Diaclone or Abcam) and then with the following secondary antibodies: goat anti-human IgG (H+L) Alexafluor 488 (Invitrogen, 1/200), goat anti-mouse IgG2b Alexafluor 647 (Invitrogen, 1/200) and goat anti-mouse IgG1 Alexafluor 568 (Invitrogen, 1/200).

## 4.9 | EV immunoprecipitation

For EV immunoprecipitation, the material corresponding to  $1 \times 10^9$  EVs isolated in F7-11 was used for each sample. Exosome Isolation kit beads (Miltenyi) were used following manufacturer's instructions. Briefly, EVs in F7-11 were incubated with 50  $\mu\text{l}$  of anti-CD63 or anti-CD9 beads overnight at 4°C. The day after, washes were performed on the columns using the isolation buffer provided in the kit. After addition of magnetically labelled EVs on columns, flow-through (FT) was recovered in the resulting running liquid which was pooled with the first wash of beads. Collected FT were then subjected to ultracentrifugation for 2 h at 125,000 g using the TLA 45 rotor (Beckman Coulter) and resuspended in 20  $\mu\text{l}$  of Laemmli 1X (BioRad). Elution of immunoprecipitated (IP) EVs was performed with 25  $\mu\text{l}$  Laemmli 1.5X. All the recovered materials of IP and FT were loaded on gels.

## 4.10 | EV analysis by bead-based multiplex flow cytometry assay

EV-R fractions were subjected to bead-based multiplex analysis by flow cytometry (MACSPlex Exosome Kit, human, Miltenyi). Samples were processed according to manufacturer instructions. The same amount ( $0.85\text{--}1.7 \times 10^9$  EVs from DMSO- or Homosalate- or Bafilomycin A1-treated MDA-MB-231 cells) were diluted with MACSPlex buffer to a final volume of 120  $\mu\text{l}$  and 15  $\mu\text{l}$  of MACSPlex Exosome Capture Beads were added. Samples were incubated on an orbital shaker overnight at room temperature protected from light. After washing, detection antibodies (APC-conjugated anti-CD9/anti-CD63/ anti-CD81 mix at dilution recommended by provider, or 5  $\mu\text{l}$  anti-SLC3A2/CD98-APC (clone REA387, MiltenyiBiotec) were incubated for 1 h at RT. Flow cytometric analysis was performed with Aurora Analyzer (Cytek) and data analysed with FlowJo software (v10, FlowJo LLC). The 39 single bead populations were gated to allow the determination of the APC signal intensity on the respective bead population. Median fluorescence intensity (MFI) for each capture bead was background corrected by dividing respective MFI values from matched non-EV controls that were treated exactly like EV-containing samples.

## 4.11 | Transmission electron microscopy (TEM)

Electron microscopy was performed on EVs isolated in F7-11 from same number of secreting cells (Figure 1F-G:  $7 \times 10^6$ , Figure 4C:  $2.7 \times 10^6$ ) and stored at  $-80^\circ\text{C}$  that had never been thawed and re-frozen. F7-11 was deposited on formvar/carbon-coated copper/palladium grids and adsorbed for 20 min before uranyl/acetate contrasting and methyl-cellulose embedding for whole-mount analysis as described previously (Théry, Amigorena, Raposo, & Clayton, 2006). Staining with CD63 or CD9 antibodies was performed according to the Protein A-gold method (Slot & Geuze, 2007) on EVs adsorbed to formvar/carbon-coated copper/palladium grids. CD63 staining was performed by incubating with mouse anti-CD63 (TS63 Diaclone 857.770.000 1/200) in

PBS-BSA 1% for 30 min and CD9 staining was performed incubating with rabbit anti-CD9 (Abcam ab236630 1/80) for 30 min, 10 nm protein-A-gold (CMC, Utrecht, The Netherlands) for 20 min, fixed for 5 min with 1% glutaraldehyde (Electron Microscopy Sciences).

Subsequently, after a wash on 10 droplets of distilled water, grids were transferred to droplets of 0.4% (w/v) uranyl acetate (UA) staining and 1.8% (w/v) methylcellulose embedding solution. After 10 min of incubation, grids were picked up in a wire loop. Most of the excess of the viscous embedding solution was drained away with filter paper after which the grids were air-dried forming a thin layer of embedding solution. Images were acquired with a digital camera Quemesa (EMSIS GmbH, Münster, Germany) mounted on a Tecnai Spirit transmission electron microscope (FEI Company) operated at 80 kV. EVs concentrations were estimated from digital images by counting the number of EVs per  $\mu\text{m}^2$ . This was performed by using the ImageJ software.

#### 4.12 | EV uptake assay

Parental MDA-MB-231 acceptor cells were seeded 24 h before the uptake experiment, at 20,000 cells per well in a 96-well plate. Cells were treated with 0.1% DMSO or 10  $\mu\text{M}$  Homosalate for 24 h, or 100 nM Bafilomycin A1 for 16 h, and fed with  $3 \times 10^7$  EVs/well from Nluc-CD9 MDA-MB-231 cells in L15 medium for the last 2 h or 16 h at 37°C. After incubation, cells were washed three times with PBS, 50  $\mu\text{l}$  of Nano-Glo reagent (Promega, Wisconsin, USA) was added on each well and luminescence activity was read using iD3 SpectraMax microplate reader (Molecular Devices, California, USA).

#### 4.13 | xCELLigence-based in vitro proliferation and resistance to anchorage loss assays

MCF7 recipient cells were seeded in 24 well plates at the density of 150,000 cells. After 24 h, cells were washed 1X with PBS and serum free DMEM containing EVs was incubated on cells during 1 h. The material corresponding to  $5 \times 10^8$  EVs isolated in F7-11 from MDA-MB-231 cells was used. After this time, cells were harvested by trypsinization. For proliferation assay, cells were resuspended in DMEM with 10% of FCS and transferred into xCELLigence microplates (E-plate 16, Agilent) at the density of 20,000 cells for real-time analysis of cell adhesion and growth. Plates were loaded into xCELLigence RTCA DP instrument (Agilent) inside a 37°C incubator. A run of 50 h with readings of impedance every 30 min was programmed. Cell-sensor impedance is expressed as an arbitrary unit called the Cell Index (CI). The CI at each time point is defined as  $(R_n - R_b)/15$ , where  $R_n$  is the cell-electrode impedance of the well when it contains cells, and  $R_b$  is the background impedance of the well with the media alone. Slopes of the cell impedance in the range 10–40h were calculated using Roche RTA software.

For the in vitro anchorage-loss assay, cells collected after trypsinization were resuspended in serum free DMEM containing 0.1% BSA and kept on ultra-low attachment (ULA) six-well plates (Corning, #3471) for 24 h. Next, cells were collected and washed with PBS, treated for 5 min with trypsin for the disruption of cell aggregates and 1/8<sup>th</sup> of the cells collected from each well were transferred into a well of xCELLigence microplates following the same procedure described for proliferation assay.

#### 4.14 | Cell survival and apoptosis assays

##### Resazurin-based dose-finding method

For resistance to apoptosis or cell death induction, a dose-response curve of Staurosporine (Sigma-Aldrich) on MCF7 was first performed to identify an intermediate concentration resulting in 60% cell viability (Figure S5A). MCF7 cells were seeded on 96-well plates (4,000 cells per well) and treated with increasing concentrations of Staurosporine in DMEM medium containing 10% FBS. Cell viability was assessed 24 h after treatment by replacing the cell culture medium with 0.004% Resazurin (Sigma-Aldrich) solution in PBS, sterile filtered, as an indicator of viable cells. After 5h incubation, reduced Resazurin, called Resorufin, was detected using the fluorescence mode (Ex/Em 530–560/590 nm) on a SpectraMax iD3 instrument. Cell viability was normalized using untreated cells as 100% cell viability and no cells as 0%.

##### ApoLive-Glo multiplex assay

MCF7 recipient cells were seeded in 24 well plates at 150,000 cells/well. After 24 h, cells were washed 1X with PBS and serum free DMEM containing EVs was incubated on cells during 1 h. The material corresponding to  $5 \times 10^8$  EVs isolated in F7-11 from MDA-MB-231 cells was used. After EV incubation, MCF7 cells were trypsinized and seeded in duplicates on white bottom 96-well Nunclon Delta plates (10,000 cells per well) and treated with Staurosporine at 33.3 nM (Cell viability IC60, 24h) or 1  $\mu\text{M}$  (Caspase activity, 6 h) in DMEM medium containing 10% FBS. For anchorage-loss experiments 10,000 MCF7 cells were plated

in parallel on regular (attachment) or on untreated (low-attachment) 96-well white bottom Nunc plates in DMEM containing 0.1% BSA for 6 h or 24 h.

Cell viability was determined by addition of a cell-permeable fluorogenic substrate (Glycyl-Phenylalanyl-Amino fluorocoumarin GF-AFC) which is activated by proteases of living cells. Caspase3/7 activity was measured by addition of a luminogenic substrate (tetrapeptide DEVD containing) that is cleaved in the presence of active Caspase3/7 in lysed cells. Fluorescence and luminescence measurements were performed 1 h after substrate addition on a SpectraMax iD3 instrument according to the manufacturer's protocol.

#### 4.15 | Wound healing assay

Migratory capacity of the MCF7 cells was examined by seeding  $3 \times 10^6$  cells in each well of a 24-well plate 24 h before the experiment. The cells were incubated with  $2 \times 10^9$  DMSO- or Homosalate- or Bafilomycin-EVs/well at 37 °C for 1 h and then a scratch was done in the middle of each well with a P200 pipette tip. After incubation, cells were washed 1 time with PBS and replenished with 10% EV-depleted serum-containing medium. Cell migration was monitored using time-lapse microscopy (IncuCyte Live Cell Analysis Systems, 4x objective lens, Sartorius) with an interval of 3 h during 21 h. Image analysis was performed with ImageJ automated by a macro: the wound area at the different time points was measured after using a variance filter to define the wound.

#### 4.16 | Statistical analysis

Following the recommendation of D.L.Vaux (Vaux, 2012), for each experiment where number of biological replicates were two or three, we displayed the results in a transparent manner, showing each individual biological replicate as a dot, so the readers could interpret the data for themselves. We (as suggested by D.L. Vaux) considered that same trends of results obtained independently 2–3 times were as informative as statistical tests to evaluate reproducibility of the experiments. Nonetheless, we also performed statistical analyses with GraphPad Prism version 8.0.2 (GraphPad software, California USA), by paired t-test (Figure 3B; Figure 4B; Figure 5A, Figure S3B, Figure S4C, Figure S5A–C), unpaired multiple t-test (Figure 5C), Mann-Whitney test (Figure 4C), ordinary one way ANOVA (Figures 3A–D, 4E, 5E, 6A, B, D) Kruskal-Wallis test (Figure 4F) and two way ANOVA (Figure 4G, 5F).

#### ACKNOWLEDGEMENTS

We thank for fruitful discussions several team members, specially Drs Mercedes Tkach, Mathilde Mathieu and Emeline Bonsergent, as well as Federico Coccozza, Davinia Arguedas and Alix Zhou, and for helpful discussions and tools Drs Michael Boutros and Alena Ivanova (DKFZ, Germany), Dr Michael Davidson (The Florida State University, USA), Dr Walter Mothes (Yale University School of Medicine, USA), Dr Mathieu Maurin (Institut Curie, France), Dr Eric Rubinstein (Centre d'Immunologie et des Maladies Infectieuses, France) and Dr. Pascale Zimmermann (Centre de Recherche en Cancerologie de Marseille, France and KU Leuven, Leuven, Belgium). We also acknowledge the following platforms of Institut Curie: PICT-IBiSA, member of the France-BioImaging national research infrastructure (ANR-10-INBS-04) for fluorescence and electron microscopy, the genomic platform for the authentication of cell lines by STR, the Extracellular Vesicle platform for MacsPlexExo analysis. This work was funded by INSERM, CNRS, Institut Curie, French IdEx and LabEx (ANR-10-IDEX-0001-02 PSL, ANR-10-LABX-0038, ANR-11-LABX-0043, ANR-18-IDEX-0001 Université de Paris), grants from french ANR (ANR-18-CE13-0017-03; ANR-18-CE15-0008-01; ANR-18-CE16-0022-02), INCa (INCA-11548), Fondation ARC (PGA1 RF20180206962), FRM (SPF20170938694), USA NIDA (DA040385). The BioPhenics laboratory is supported by Institut Curie, IBiSA (PICT-IBiSA) and part of ChemBioFRance and France-BioImaging national infrastructures. SD was supported by a EMBO Scientific exchange grant (SEG9045).

#### AUTHOR CONTRIBUTIONS

Eleonora Grisard, Lorena Martin-Jaular and Clotilde Théry designed the study, interpreted the data, wrote the article. Elaine Del Nery contributed to screening design and implementation. Eleonora Grisard, Nathalie Nevo, Sebastian Doll, Aurianne Lescure, Mabel Jouve performed experiments. Maxime Corbé designed and implemented the computational framework to analyse the screening data. Eleonora Grisard, Nathalie Nevo, Sebastian Doll, Aurianne Lescure, Maxime Corbé, Mabel Jouve analysed the data. Eleonora Grisard, Alain Joliot, Gregory Lavieuv generated plasmids or cells. Alain Joliot and Elaine Del Nery interpreted data. All authors read and corrected the article.

#### CONFLICT OF INTEREST

The authors declare no conflict of interest.

## ORCID

Eleonora Grisard  <https://orcid.org/0000-0002-4585-9244>  
 Nathalie Nevo  <https://orcid.org/0000-0001-6350-7122>  
 Sebastian Doll  <https://orcid.org/0000-0002-8933-5362>  
 Mabel Jouve  <https://orcid.org/0000-0002-3115-4681>  
 Gregory Lavieu  <https://orcid.org/0000-0001-9852-4977>  
 Alain Joliot  <https://orcid.org/0000-0002-2215-1550>  
 Elaine Del Nery  <https://orcid.org/0000-0002-9654-5202>  
 Lorena Martin-Jaular  <https://orcid.org/0000-0002-1511-8576>  
 Clotilde Théry  <https://orcid.org/0000-0001-8294-6884>

## REFERENCES

- Alamer, M., & Darbre, P. D. (2018). Effects of exposure to six chemical ultraviolet filters commonly used in personal care products on motility of MCF-7 and MDA-MB-231 human breast cancer cells in vitro. *Journal of Applied Toxicology*, 38(2), 148–159. <https://doi.org/10.1002/jat.3525>
- Auld, D. S., & Inglese, J. (2016). Interferences with Luciferase Reporter Enzymes. In S. Markossian (Eds.) et. al., *Assay Guidance Manual Eli Lilly & Company and the National Center for Advancing Translational Sciences*, 1(Md), 1–13. Available: <http://www.ncbi.nlm.nih.gov/pubmed/27478246>
- Auld, D. S., Narahari, J., Ho, P.-I., Casalena, D., Nguyen, V., Cirbaite, E., Hughes, D., Daly, J., & Webb, B. (2018). Characterization and use of turboluciferase as a reporter for high-throughput assays. *Biochemistry*, 57(31), 4700–4706. <https://doi.org/10.1021/acs.biochem.8b00290>
- Bebelmann, M. P., Bun, P., Huvencuers, S., van Niel, G., Pegtel, D. M., & Verweij, F. J. (2020). Real-time imaging of multivesicular body–plasma membrane fusion to quantify exosome release from single cells. *Nature Protocols*, 15(1), 102–121. <https://doi.org/10.1038/s41596-019-0245-4>
- Birmingham, A., Selfors, L. M., Forster, T., Wrobel, D., Kennedy, C. J., Shanks, E., Santoyo-Lopez, J., Dunican, D. J., Long, A., Kelleher, D., Smith, Q., Beijersbergen, R. L., Ghazal, P., & Shamu, C. E. (2009). Statistical methods for analysis of high-throughput RNA interference screens. *Nature Methods*, 6(8), 569–575. <https://doi.org/10.1038/nmeth.1351>
- Böing, A. N., Van Der Pol, E., Grootemaat, A. E., Coumans, F. A. W., Sturk, A., & Nieuwland, R. (2014). Single-step isolation of extracellular vesicles by size-exclusion chromatography. *Journal of Extracellular Vesicles*, 3(1), 23430. <https://doi.org/10.3402/jev.v3.23430>
- Bolte, S., & Cordelières, F. P. (2006). A guided tour into subcellular colocalization analysis in light microscopy. *Journal of Microscopy*, 224(3), 213–232. <https://doi.org/10.1111/j.1365-2818.2006.01706.x>
- Bonsergent, E., Grisard, E., Buchrieser, J., Schwartz, O., Théry, C., & Lavieu, G. (2021). Quantitative characterization of extracellular vesicle uptake and content delivery within mammalian cells. *Nature Communication*, 12(1), 1864. <https://doi.org/10.1038/s41467-021-22126-y>
- Bowman, E. J., Siebers, A., & Altendorf, K. (1988). Bafilomycins; A class of inhibitors of membrane ATPases from microorganisms, animal cells, and plant cells. *PNAS*, 85(21), 7972–7976. <https://doi.org/10.1073/pnas.85.21.7972>
- Carlsson, S. R., Roth, J., Piller, F., & Fukuda, M. (1988). Isolation and characterization of human lysosomal membrane glycoproteins, h-lamp-1 and h-lamp-2. Major sialoglycoproteins carrying polylectosaminoglycan. *Journal of Biological Chemistry*, 263(35), 18911–18919. [https://doi.org/10.1016/s0021-9258\(18\)37369-1](https://doi.org/10.1016/s0021-9258(18)37369-1)
- Cashikar, A. G., & Hanson, P. I. (2019). A cell-based assay for CD63-containing extracellular vesicles. *Plos One*, 14(7), e0220007. <https://doi.org/10.1371/journal.pone.0220007>
- Chung, N., Zhang, X. D., Kreamer, A., Locco, L., Kuan, P.-F., Bartz, S., Linsley, P. S., Ferrer, M., & Strulovici, B. (2008). Median absolute deviation to improve hit selection for genome-scale RNAi screens. *Journal of Biomolecular Screening: The Official Journal of the Society for Biomolecular Screening*, 13(2), 149–158. <https://doi.org/10.1177/1087057107312035>
- Ciardello, C., Leone, A., Lanuti, P., Roca, M. S., Moccia, T., Minciacci, V. R., Minopoli, M., Gigantino, V., De Cecio, R., Rippa, M., Petti, L., Capone, F., Vitagliano, C., Milone, M. R., Pucci, B., Lombardi, R., Iannelli, F., Di Gennaro, E., Bruzzese, F., & ... Budillon, A. (2019). Large oncosomes overexpressing integrin alpha-V promote prostate cancer adhesion and invasion via AKT activation. *Journal of Experimental & Clinical Cancer Research*, 38, 317. <https://doi.org/10.1186/s13046-019-1317-6>
- Cocozza, F., Grisard, E., Martin-Jaular, L., Mathieu, M., & Théry, C. (2020). SnapShot: Extracellular vesicles. *Cell*, 182(1), 262–262.e1. <https://doi.org/10.1016/j.cell.2020.04.054>
- Costa-Silva, B., Aiello, N. M., Ocean, A. J., Singh, S., Zhang, H., Thakur, B. K., Becker, A., Hoshino, A., Mark, M. T., Molina, H., Xiang, J., Zhang, T., Theilen, T.-M., Garcia-Santos, G., Williams, C., Ararso, Y., Huang, Y., Rodrigues, G., Shen, T.-L., & ... Lyden, D. (2015). Pancreatic cancer exosomes initiate pre-metastatic niche formation in the liver. *Nature Cell Biology*, 17(6), 816–826. <https://doi.org/10.1038/ncb3169>
- Couteau, C., Chauvet, C., Papis, E., & Coiffard, L. (2012). UV filters, ingredients with a recognized anti-inflammatory effect. *Plos One*, 7(12), 2–7. <https://doi.org/10.1371/journal.pone.0046187>
- Crowley, L. C., Marfell, B. J., & Waterhouse, N. J. (2016). Analyzing cell death by nuclear staining with Hoechst 33342. *Cold Spring Harbor Protocols*, 2016(9), 778–781. <https://doi.org/10.1101/pdb.prot087205>
- Datta, A., Kim, H., Lal, M., Mcgee, L., Johnson, A., Moustafa, A. A., Jones, J. C., Mondal, D., Ferrer, M., & Abdel-Mageed, A. B. (2017). Manumycin A suppresses exosome biogenesis and secretion via targeted inhibition of Ras/Raf/ERK1/2 signaling and hnRNP H1 in castration-resistant prostate cancer cells. *Cancer Letters*, 408, 73–81. <https://doi.org/10.1016/j.canlet.2017.08.020>
- Edgar, J. R., Manna, P. T., Nishimura, S., Banting, G., & Robinson, M. S. (2016). Tetherin is an exosomal tether. *Elife*, 5(September), e17180. <https://doi.org/10.7554/eLife.17180>
- Eitan, E., Suire, C., Zhang, S., & Mattson, M. P. (2016). Impact of lysosome status on extracellular vesicle content and release. *Ageing Research Reviews*, 32, 65–74. <https://doi.org/10.1016/j.arr.2016.05.001>
- Fang, T., Lv, H., Lv, G., Li, T., Wang, C., Han, Q., Yu, L., Su, B. O., Guo, L., Huang, S., Cao, D., Tang, L., Tang, S., Wu, M., Yang, W., & Wang, H. (2018). Tumor-derived exosomal miR-1247-3p induces cancer-associated fibroblast activation to foster lung metastasis of liver cancer. *Nature Communication*, 9(1), 191. <https://doi.org/10.1038/s41467-017-02583-0>
- Fong, M. Y., Zhou, W., Liu, L., Alontaga, A. Y., Chandra, M., Ashby, J., Chow, A., O'connor, S. T. F., Li, S., Chin, A. R., Somlo, G., Palomares, M., Li, Z., Tremblay, J. R., Tsuyada, A., Sun, G., Reid, M. A., Wu, X., Swiderski, P., & ... Wang, S. E. (2015). Breast-cancer-secreted miR-122 reprograms glucose metabolism in premetastatic niche to promote metastasis. *Nature Cell Biology*, 17(2), 183–194. <https://doi.org/10.1038/ncb3094>
- Frisch, S. M., & Screaton, R. A. (2001). Anoikis mechanisms. *Current Opinion in Cell Biology*, 13(5), 555–562. [https://doi.org/10.1016/S0955-0674\(00\)00251-9](https://doi.org/10.1016/S0955-0674(00)00251-9)

- Frisch, S. M., & Francis, H. (1994). Disruption of epithelial cell-matrix interactions induces apoptosis. *Journal of Cell Biology*, 124(4), 619–626. <https://doi.org/10.1083/jcb.124.4.619>
- Ghossoub, R., Lembo, F., Rubio, A., Gaillard, C. B., Bouchet, J., Vitale, N., Slavík, J., Machala, M., & Zimmermann, P. (2014). Syntenin-ALIX exosome biogenesis and budding into multivesicular bodies are controlled by ARF6 and PLD2. *Nature Communication*, 5(1), 3477. <https://doi.org/10.1038/ncomms4477>
- Haemmerle, M., Taylor, M. L., Gutschner, T., Pradeep, S., Cho, M. S., Sheng, J., Lyons, Y. M., Nagaraja, A. S., Dood, R. L., Wen, Y., Mangala, L. S., Hansen, J. M., Rupaimoole, R., Gharpure, K. M., Rodriguez-Aguayo, C., Yim, S. Y., Lee, J.-S., Ivan, C., Hu, W., & ... Sood, A. K. (2017). Platelets reduce anoikis and promote metastasis by activating YAP1 signaling. *Nature Communication*, 8(1), 310. <https://doi.org/10.1038/s41467-017-00411-z>
- Hall, M. P., Unch, J., Binkowski, B. F., Valley, M. P., Butler, B. L., Wood, M. G., Otto, P., Zimmerman, K., Vidugiris, G., Machleidt, T., Robers, M. B., Benink, H. A., Eggers, C. T., Slater, M. R., Meisenheimer, P. L., Klaubert, D. H., Fan, F., Encell, L. P., & Wood, K. V. (2012). Engineered luciferase reporter from a deep sea shrimp utilizing a novel imidazopyrazinone substrate. *ACS Chemical Biology*, 7(11), 1848–1857. <https://doi.org/10.1021/cb3002478>
- Ho, P.-I., Yue, K., Pandey, P., Breault, L., Harbinski, F., Mcbride, A. J., Webb, B., Narahari, J., Karassina, N., Wood, K. V., Hill, A., & Auld, D. S. (2013). Reporter enzyme inhibitor study to aid assembly of orthogonal reporter gene assays. *ACS Chemical Biology*, 8(5), 1009–1017. <https://doi.org/10.1021/cb3007264>
- Iglewicz, B., & Hoaglin, D. C. (1993). *Volume 16: How to Detect and Handle Outliers, The ASQC Basic References in Quality Control: Statistical Techniques, 16*, 1–85.
- Imjeti, N. S., Menck, K., Egea-Jimenez, A. L., Lecointre, C., Lembo, F., Bouguenina, H., Badache, A., Ghossoub, R., David, G., Roche, S., & Zimmermann, P. (2017). Syntenin mediates SRC function in exosomal cell-to-cell communication. *PNAS*, 114(47), 12495–12500. <https://doi.org/10.1073/pnas.1713433114>
- Jeppesen, D. K., Fenix, A. M., Franklin, J. L., Higginbotham, J. N., Zhang, Q., Zimmerman, L. J., Liebler, D. C., Ping, J., Liu, Q., Evans, R., Fissell, W. H., Patton, J. G., Rome, L. H., Burnette, D. T., & Coffey, R. J. (2019). Reassessment of exosome composition. *Cell*, 177(2), 428–445.e18. <https://doi.org/10.1016/j.cell.2019.02.029>
- Kia, V., Mortazavi, Y., Paryan, M., Biglari, A., & Mohammadi-Yeganeh, S. (2019). Exosomal miRNAs from highly metastatic cells can induce metastasis in non-metastatic cells. *Life Sciences*, 220(January), 162–168. <https://doi.org/10.1016/j.lfs.2019.01.057>
- Kim, H., Sung, J. Y., Park, E.-K., Kho, S., Koo, K. H., Park, S.-Y., Goh, S.-H., Jeon, Y. K., Oh, S., Park, B.-K., Jung, Y.-K., & Kim, Y.-N. (2017). Regulation of anoikis resistance by NADPH oxidase 4 and epidermal growth factor receptor. *British Journal of Cancer*, 116(3), 370–381. <https://doi.org/10.1038/bjc.2016.440>
- Koliha, N., Wienczek, Y., Heider, U., Jüngst, C., Kladt, N., Krauthäuser, S., & Wild, S. (2016). A novel multiplex bead-based platform highlights the diversity of extracellular vesicles Cologne Excellence Cluster on Cellular Stress Responses in Aging-Associated Diseases. *Journal of Extracellular Vesicles*, 1(17), 29975.
- Kowal, J., Arras, G., Colombo, M., Jouve, M., Morath, J. P., Prindal-Bengtson, B., Dingli, F., Loew, D., Tkach, M., & Théry, C. (2016). Proteomic comparison defines novel markers to characterize heterogeneous populations of extracellular vesicle subtypes. *Proceedings of the National Academy of Sciences*, 113(8), E968–E977. <https://doi.org/10.1073/pnas.1521230113>
- Krämer-Albers, E.-M., Bretz, N., Tenzer, S., Winterstein, C., Möbius, W., Berger, H., Nave, K.-A., Schild, H., & Trotter, J. (2007). Oligodendrocytes secrete exosomes containing major myelin and stress-protective proteins: Trophic support for axons?. *Proteomics. Clinical applications*, 1(11), 1446–1461. <https://doi.org/10.1002/prca.200700522>
- Krause, M., Klit, A., Blomberg Jensen, M., Søeborg, T., Frederiksen, H., Schlumpf, M., Lichtensteiger, W., Skakkebaek, N. E., & Drzewiecki, K. T. (2012). Sunscreens: Are they beneficial for health? An overview of endocrine disrupting properties of UV-filters. *International Journal of Andrology*, 35(3), 424–436. <https://doi.org/10.1111/j.1365-2605.2012.01280.x>
- Lázaro-Ibáñez, E., Faruqi, F. N., Saleh, A. F., Silva, A. M., Tzu-Wen Wang, J., Rak, J., Al-Jamal, K. T., & Dekker, N. (2021). Selection of fluorescent, bioluminescent, and radioactive tracers to accurately reflect extracellular vesicle biodistribution in vivo. *ACS Nano*, 15(2), 3212–3227. <https://doi.org/10.1021/acsnano.0c09873>
- Leblanc, R., Kashyap, R., Barral, K., Egea-Jimenez, A. L., Kovalskyy, D., Feracci, M., Garcia, M., Derviaux, C., Betzi, S., Ghossoub, R., Platonov, M., Roche, P., Morelli, X., Hoffer, L., & Zimmermann, P. (2020). Pharmacological inhibition of syntenin PDZ2 domain impairs breast cancer cell activities and exosome loading with syndecan and EpCAM cargo. *Journal of Extracellular Vesicles*, 10(2), e12039. <https://doi.org/10.1002/jev2.12039>
- Li, B., Antonyak, M. A., Zhang, J., & Cerione, R. A. (2012). RhoA triggers a specific signaling pathway that generates transforming microvesicles in cancer cells. *Oncogene*, 31(45), 4740–4749. <https://doi.org/10.1038/nc.2011.636>
- Macarron, R., Banks, M. N., Bojanic, D., Burns, D. J., Cirovic, D. A., Garyantes, T., Green, D. V. S., Hertzberg, R. P., Janzen, W. P., Paslay, J. W., Schopfer, U., & Sittampalam, G. S. (2011). Impact of high-throughput screening in biomedical research. *Nature reviews. Drug discovery*, 10(3), 188–195. <https://doi.org/10.1038/nrd3368>
- Mathieu, M., Névo, N., Jouve, M., Valenzuela, J. I., Maurin, M., Verweij, F. J., Palmulli, R., Lankar, D., Dingli, F., Loew, D., Rubinstein, E., Boncompain, G., Perez, F., & Théry, C. (2021). Specificities of exosome versus small ectosome secretion revealed by live intracellular tracking and synchronized extracellular vesicle release of CD9 and CD63. *Nature Communication*, 12(1), 4389. <https://doi.org/10.1038/s41467-021-24384-2>
- Minciacchi, V. R., Freeman, M. R., & Di Vizio, D. (2015). Extracellular vesicles in cancer: exosomes, microvesicles and the emerging role of large oncosomes. *Seminars in cell & developmental biology*, 40, 41–51. <https://doi.org/10.1016/j.semcdb.2015.02.010>
- Mosteller, F., & Tukey, J. W. (1977). *Data analysis and regression*. Addison-Wesley Pub. Co.
- Muralidharan-Chari, V., Clancy, J., Plou, C., Romao, M., Chavrier, P., Raposo, G., & D'souza-Schorey, C. (2009). ARF6-regulated shedding of tumor cell-derived plasma membrane microvesicles. *Current Biology*, 19(22), 1875–1885. <https://doi.org/10.1016/j.cub.2009.09.059>
- Nolte-T Hoen, E., Cremer, T., Gallo, R. C., & Margolis, L. B. (2016). Extracellular vesicles and viruses: Are they close relatives?. *PNAS*, 113(33), 9155–9161. <https://doi.org/10.1073/pnas.1605146113>
- Opinion, P. (2020). Scientific Committee on Consumer Safety SCCS OPINION on Homosalate. no. October. Available: [https://ec.europa.eu/health/sites/health/files/scientific\\_committees\\_consumer\\_safety/docs/sccs\\_o\\_244.pdf](https://ec.europa.eu/health/sites/health/files/scientific_committees_consumer_safety/docs/sccs_o_244.pdf)
- Otsu, N. (1979). Threshold selection method from gray-level histograms. *Ieee Transactions on Systems, Man, and Cybernetics*, 20(1), 62–66.
- Paoli, P., Giannoni, E., & Chiarugi, P. (2013). Anoikis molecular pathways and its role in cancer progression. *Biochimica et Biophysica Acta - Molecular and Cellular Research*, 1833(12), 3481–3498. <https://doi.org/10.1016/j.bbamcr.2013.06.026>
- Plebanek, M. P., Angeloni, N. L., Vinokour, E., Li, J., Henkin, A., Martinez-Marin, D., Filleur, S., Bhowmick, R., Henkin, J., Miller, S. D., Ifergan, I., Lee, Y., Osman, I., Thaxton, C. S., & Volpert, O. V. (2017). Pre-metastatic cancer exosomes induce immune surveillance by patrolling monocytes at the metastatic niche. *Nature Communication*, 8(1), 1319. <https://doi.org/10.1038/s41467-017-01433-3>
- Rous, B. A., Reaves, B. J., Ihrke, G., Briggs, J. A. G., Gray, S. R., Stephens, D. J., Banting, G., & Luzio, J. P. (2002). Role of adaptor complex AP-3 in targeting wild-type and mutated CD63 to lysosomes. *Molecular Biology of the Cell*, 13(3), 1071–1082. <https://doi.org/10.1091/mbc.01-08-0409>
- Seiler, A., Schneider, M., Förster, H., Roth, S., Wirth, E. K., Culmsee, C., Plesnila, N., Kremmer, E., Rådmark, O., Wurst, W., Bornkamm, G. W., Schweizer, U., & Conrad, M. (2008). Glutathione peroxidase 4 senses and translates oxidative stress into 12/15-lipoxygenase dependent- and AIF-mediated cell death. *Cell Metabolism*, 8(3), 237–248. <https://doi.org/10.1016/j.cmet.2008.07.005>
- Shpigelman, J., Lao, F. S., Yao, S., Li, C., Saito, T., Sato-Kaneko, F., Nolan, J. P., Shukla, N. M., Pu, M., Messer, K., Cottam, H. B., Carson, D. A., Corr, M., & Hayashi, T. (2021). Generation and application of a reporter cell line for the quantitative screen of extracellular vesicle release. *Frontiers in Pharmacology*, 12, 668609. <https://doi.org/10.3389/fphar.2021.668609>

- Slot, J. W., & Geuze, H. J. (2007). Cryosectioning and immunolabeling. *Nature Protocols*, 2(10), 2480–2491. <https://doi.org/10.1038/nprot.2007.365>
- Théry, C., Amigorena, S., Raposo, G., & Clayton, A. (2006). Isolation and characterization of exosomes from cell culture supernatants and biological fluids. *Current Protocols in Cell Biology*, 30(1), 3–22. <https://doi.org/10.1002/0471143030.cb0322s30>
- Théry, C., Witwer, K. W., Aikawa, E., Alcaraz, M. J., Anderson, J. D., Andriantsitohaina, R., Antoniou, A., Arab, T., Archer, F., Atkin-Smith, G. K., Ayre, D. C., Bach, J.-M., Bachurski, D., Baharvand, H., Balaj, L., Baldacchino, S., Bauer, N. N., Baxter, A. A., Bebawy, M., & ... Zuba-Surma, E. K. (2018). Minimal information for studies of extracellular vesicles 2018 (MISEV2018): A position statement of the International Society for Extracellular Vesicles and update of the MISEV2014 guidelines. *Journal of extracellular vesicles*, 7(1), 1535750. <https://doi.org/10.1080/20013078.2018.1535750>
- Tkach, M., Thalmensi, J., Timperi, E., Gueguen, P., Névo, N., Grisard, E., & Théry, C. (2022). Extracellular vesicles from triple negative breast cancer promote pro-inflammatory macrophages associated with better clinical outcome. *PNAS*, 119(17), e2107394119. <https://doi.org/10.1073/pnas.2107394119>
- Tkach, M., & Théry, C. (2016). Communication by extracellular vesicles: Where we are and where we need to go. *Cell*, 164(6), 1226–1232. <https://doi.org/10.1016/j.cell.2016.01.043>
- Trajkovic, K., Hsu, C., Chiantia, S., Rajendran, L., Wenzel, D., Wieland, F., & Simons, M. (2008). Ceramide triggers budding of exosome vesicles into multivesicular endosomes. *Science* (80), 320(5873), 179. <https://doi.org/10.1126/science.320.5873.179>
- van Deun, J., Mestdagh, P., Agostinis, P., Akay, Ö., Anand, S., Anckaert, J., Martinez, Z. A., Baetens, T., Beghein, E., Bertier, L., Berx, G., Boere, J., Boukouris, S., Bremer, M., Buschmann, D., Byrd, J. B., Casert, C., Cheng, L., Cmoch, A., & ... Hendrix, A. (2017). EV-TRACK: Transparent reporting and centralizing knowledge in extracellular vesicle research. *Nature Methods*, 14(3), 228–232. <https://doi.org/10.1038/nmeth.4185>
- Van Niel, G., D'Angelo, G., & Raposo, G. (2018). Shedding light on the cell biology of extracellular vesicles. *Nature Reviews Molecular Cell Biology*, 19(4), 213–228. <https://doi.org/10.1038/nrm.2017.125>
- Vaux, D. L. (2012). Research methods: Know when your numbers are significant. *Nature*, 492(7428), 180–181. <https://doi.org/10.1038/492180a>
- Wang, Y., Marling, S. J., Plum, L. A., & Deluca, H. F. (2017). Salate derivatives found in sunscreens block experimental autoimmune encephalomyelitis in mice. *PNAS*, 114(32), 8528–8531. <https://doi.org/10.1073/pnas.1703995114>
- Wang, Y.-N., Zeng, Z.-L., Lu, J., Wang, Y., Liu, Z.-X., He, M.-M., Zhao, Q., Wang, Z.-X., Li, T., Lu, Y.-X., Wu, Q.-N., Yu, K., Wang, F., Pu, H.-Y., Li, B., Jia, W.-H., Shi, M., Xie, D., Kang, T.-B., & ... Xu, R.-H. (2018). CPT1A-mediated fatty acid oxidation promotes colorectal cancer cell metastasis by inhibiting anoikis. *Oncogene*, 37(46), 6025–6040. <https://doi.org/10.1038/s41388-018-0384-z>
- Willms, E., Cabañas, C., Mäger, I., Wood, M. J. A., & Vader, P. (2018). Extracellular vesicle heterogeneity: Subpopulations, isolation techniques, and diverse functions in cancer progression. *Frontiers in Immunology*, 9, 738. <https://doi.org/10.3389/fimmu.2018.00738>
- Wolfers, J., Lozier, A., Raposo, G., Regnault, A., Théry, C., Masurier, C., Flament, C., Pouzieux, S., Faure, F., Tursz, T., Angevin, E., Amigorena, S., & Zitvogel, L. (2001). Tumor-derived exosomes are a source of shared tumor rejection antigens for CTL cross-priming. *Nature Medicine*, 38, 297–303.
- Yazar, S., & Kara Ertekin, S. (2020). Assessment of the cytotoxicity and genotoxicity of homosalate in MCF-7. *Journal of Cosmetic Dermatology*, 19(1), 246–252. <https://doi.org/10.1111/jocd.12973>
- Zhang, H., Freitas, D., Kim, H. S., Fabijanic, K., Li, Z., Chen, H., Mark, M. T., Molina, H., Martin, A. B., Bojmar, L., Fang, J., Rampersaud, S., Hoshino, A., Matei, I., Kenific, C. M., Nakajima, M., Mutvei, A. P., Sansone, P., Buehring, W., & ... Lyden, D. (2018). Identification of distinct nanoparticles and subsets of extracellular vesicles by asymmetric flow field-flow fractionation. *Nature Cell Biology*, 20(3), 332–343. <https://doi.org/10.1038/s41556-018-0040-4>
- Zhang, Y., Lu, H., Dazin, P., & Kapila, Y. (2004). Squamous cell carcinoma cell aggregates escape suspension-induced, p53-mediated anoikis: Fibronectin and integrin  $\alpha$ v mediate survival signals through focal adhesion kinase. *Journal of Biological Chemistry*, 279(46), 48342–48349. <https://doi.org/10.1074/jbc.M407953200>

## SUPPORTING INFORMATION

Additional supporting information can be found online in the Supporting Information section at the end of this article.

**How to cite this article:** Grisard, E., Nevo, N., Lescure, A., Doll, S., Corbé, M., Jouve, M., Lavieu, G., Joliot, A., Del Nery, E., Martin-Jaular, L., & Théry, C. (2022). Homosalate boosts the release of tumour-derived Extracellular Vesicles with protection against anchorage-loss property. *Journal of Extracellular Vesicles*, 11, e12242. <https://doi.org/10.1002/jev2.12242>